Neurobiology of Disease 160 (2021) 105515

Contents lists available at ScienceDirect

Neurobiology of Disease

journal homepage: www.elsevier.com/locate/ynbdi

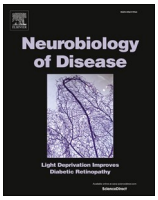

Thioridazine reverts the phenotype in cellular and *Drosophila* models of amyotrophic lateral sclerosis by enhancing TDP-43 aggregate clearance

Lucia Cragnaz [a,1], Greta Spinelli [a,1], Laura De Conti [a,1], Emilie A. Bureau [b], Janet Brownlees [b], Fabian Feiguin [a,d], Valentina Romano [a], Natasa Skoko [a], Raffaella Klima [a], Catherine A. Kettleborough [b], Francisco E. Baralle [c], Marco Baralle [a,*]

[a] International Centre for Genetic Engineering and Biotechnology (ICGEB), Padriciano 99, 34149 Trieste, Italy
[b] LifeArc, Accelerator Building, Open Innovation Campus, Stevenage SG1 2FX, United Kingdom
[c] Fondazione Italiana Fegato-Onlus, Bldg. Q, AREA Science Park, ss14, Km 163.5, Basovizza, 34149 Trieste, Italy.
[d] Department of Life and Environmental Sciences, University of Cagliari, 09042 Monserrato, Cagliari, Italy.

ARTICLE INFO

Keywords:
ALS
Aggregation
Drosophila
TBPH
TDP-43
Thioridazine
Autophagy
Ubiquitin–proteasome
Phenotypic screen

ABSTRACT

Brain inclusions mainly composed of misfolded and aggregated TAR DNA binding protein 43 (TDP-43), are characteristic hallmarks of amyotrophic lateral sclerosis (ALS). Irrespective of the role played by the inclusions, their reduction represents an important therapeutic pathway that is worth exploring. Their removal can either lead to the recovery of TDP-43 function by removing the self-templating conformers that sequester the protein in the inclusions, and/or eliminate any potential intrinsic toxicity of the aggregates. The search for curative therapies has been hampered by the lack of ALS models for use in high-throughput screening. We adapted, optimised, and extensively characterised our previous ALS cellular model for such use. The model demonstrated efficient aggregation of endogenous TDP-43, and concomitant loss of its splicing regulation function. We provided a proof-of-principle for its eventual use in high-throughput screening using compounds of the tricyclic family and showed that recovery of TDP-43 function can be achieved by the enhanced removal of TDP-43 aggregates by these compounds. We observed that the degradation of the aggregates occurs independent of the autophagy pathway beyond autophagosome-lysosome fusion, but requires a functional proteasome pathway. The in vivo translational effect of the cellular model was tested with two of these compounds in a *Drosophila* model expressing a construct analogous to the cellular model, where thioridazine significantly improved the locomotive defect. Our findings have important implications as thioridazine cleared TDP-43 aggregates and recovered TDP-43 functionality. This study also highlights the importance of a two-stage, in vitro and in vivo model system to cross-check the search for small molecules that can clear TDP-43 aggregates in TDP-43 proteinopathies.

1. Introduction

Amyotrophic lateral sclerosis (ALS) is a disease that is characterised by progressive degeneration of the motor neurons in the primary motor cortex, brainstem and spinal cord. The initial foci of pathogenesis appear at the motor neuron terminals, with retrograde axonal degeneration ultimately reaching the motor neuron soma, leading to neuronal dysfunction. This results in muscle weakness, paralysis, and death within 2–5 years of the clinical onset (Silani et al., 2017). Several pathogenic mechanisms have been proposed to account for ALS, including glutamate-induced excitotoxicity (Van Damme et al., 2005) oxidative stress (Dadon-Nachum et al., 2011), and mitochondrial dysfunction (Cozzolino and Carrì, 2012). In the last decade, however, aberrant protein aggregation has been identified as the possible initial pathological mechanism underlying non-superoxide dismutase (SOD), ALS (Ratti and Buratti, 2016). The major component of neuronal and glial ubiquitinated inclusions was identified as the TAR DNA binding protein 43 (TDP-43), which belongs to the heterogeneous nuclear ribonucleoprotein (hnRNP) family (Neumann et al., 2006). TDP-43 is now known to link the sporadic and familial forms of ALS, and causative mutations in this protein have been identified in affected individuals (Sreedharan et al., 2008). Furthermore, 40% of the patients with

* Corresponding author.
E-mail address: barallem@icgeb.org (M. Baralle).
[1] Equal contribution.

https://doi.org/10.1016/j.nbd.2021.105515
Received 17 December 2020; Received in revised form 6 August 2021; Accepted 21 September 2021
Available online 24 September 2021
0969-9961/© 2021 The Authors. Published by Elsevier Inc. This is an open access article under the CC BY-NC-ND license (http://creativecommons.org/licenses/by-nc-nd/4.0/).

frontotemporal lobar degeneration with tau-negative, ubiquitin-positive inclusions (FTLD-U) (Ling et al., 2013; Mackenzie et al., 2010) show TDP-43 containing neuronal inclusions, as do approximately one-third of Alzheimer's disease (AD) brains. TDP-43 protein deposition also occurs in other disorders (Geser et al., 2009), resulting in the term TDP-43 proteinopathies to delineate a spectrum of disorders characterised by the presence of misfolded and aggregated TDP-43 (Taylor et al., 2016).

To date, the exact pathological significance of these aggregates remains unknown. The possibilities range from the inherent toxicity of the aggregates to loss-of function-effects, owing to the sequestration of TDP-43 in the aggregates, resulting in a lack of its functional form. Both possibilities are not mutually exclusive (Lee et al., 2011). Regarding the loss-of-function effects, these occur due to the fact that TDP-43 is a nuclear RNA-binding protein that actively shuttles between the nucleus and cytoplasm (Ayala et al., 2008), areas in which it is involved in several aspects of RNA processing (Buratti and Baralle, 2012). In fact, disruption of the nuclear import pathway by knockdown of the importin subunit beta-1 leads to the cytoplasmic accumulation of TDP-43 (Nishimura et al., 2010). Moreover, in the cytoplasm, it has been implicated in the anterograde axonal transport of mRNAs (Alami et al., 2014). Therefore, mislocalization and/or changes in the functional TDP-43 levels within the cell, such as those in ALS and FTLD-U, where TDP-43 is typically lost from its normal location in the neuronal nuclei and aggregated in the cytoplasm (Neumann et al., 2006), will upset a myriad of fundamental RNA metabolic processes.

Further support for the fact that the loss of TDP-43 function is involved in the neurodegeneration observed in ALS initially came from evidence derived from evolutionarily distant but functionally related species. Human TDP-43 has been demonstrated to be functionally interchangeable with its *Drosophila* ortholog, TBPH (Ayala et al., 2005). The knockout of TBPH in *Drosophila* results in a severe locomotion defect due to the atrophy of the neuromuscular junction (Feiguin et al., 2009). Among mammalian models, the importance of this protein was demonstrated in a mouse model, in which TDP-43 knockout resulted in early embryonic lethality (Kraemer et al., 2010; Sephton et al., 2010). Knockout of TDP-43 in mouse postnatal motor neurons demonstrated the link between the loss-of-function of TDP-43 and ALS as these mice showed an age dependent progressive motor neuronal dysfunction phenotype (Iguchi et al., 2013). In ALS patients, analysis of splicing changes regulated by TDP-43 also supports a loss-of-function role for TDP-43. For example, TDP-43 represses cryptic exons to maintain a normal transcriptome (Ling et al., 2015). This was found to be impaired in post-mortem brain tissues from an ALS-FTD cohort, suggesting that this splicing defect could potentially underlie TDP-43 proteinopathy (Ling et al., 2015). Additionally, analysis of the splicing changes in a series of alternatively spliced exons regulated by TDP-43 showed that these changes vary between human ALS and control spinal cords (Yang et al., 2014). Pertinent to this study, a splicing event that is dependent on TDP-43 levels is that of *POLDIP3* exon 3. A reduction in the levels of TDP-43 via siRNA in vitro has been shown to promote the exclusion of the exon giving rise to the *POLDIP3* variant-2 (Fiesel et al., 2012). The mRNA of *POLDIP3* variant 2 was observed to be significantly increased in the thalamus, motor cortex and spinal cord of patients with ALS and controls (Shiga et al., 2012), indicating of a loss of TDP-43 in ALS.

Regarding TDP-43 overexpression, the toxicity of excess TDP-43 has been demonstrated in cells (Winton et al., 2008; Zhang et al., 2013) *and* in vivo models (Wegorzewska and Baloh, 2011). These studies also highlighted the fact that insoluble TDP-43 inclusions contributed to neurodegeneration to a lesser degree than the actual overexpression of TDP-43. In fact, on using mutations that increase hydrophobicity and aggregation of TDP-43 in yeast, the aggregates strongly reduced the toxicity of the protein (Bolognesi et al., 2019). Even through it remains to be established whether the aggregation of TDP-43 is also protective in neurons, at least in the *Drosophila* eye, TDP-43 aggregates were not toxic but were protective in the presence of excess TDP-43 (Cragnaz et al., 2014). Overexpression of TBPH in the eye results in necrosis and loss of function of the eye, this neurotoxicity could be abolished by co-expression of an aggregate inducer which incorporated TDP-43 into the insoluble aggregates and restored normal eye morphology and fly vision.

Taken together, these data indicate that it is plausible that the contribution of TDP-43 to the pathogenesis of ALS is due to the progressive sequestration of TDP-43 with consequent loss of functionality, eventually reaching a critically low level of biologically active protein that is insufficient to fulfil its functions in RNA processing and transport. In fact, the normal physiological age-related drop in the expression of *Drosophila* TBPH coincides with the onset of locomotive defective phenotype in a *Drosophila* aggregation model (Cragnaz et al., 2015). This raises the question of whether it is possible to reverse the neurological phenotypes generated by the loss-of-function, of TDP-43 by the reintroduction of TDP-43. This issue was assessed using a *Drosophila* TBPH, null-allele model, where late expression of an inducible TBPH transgene resulted in the recovery of the normal phenotype, revealing an unexpected late-stage functional and structural neuronal plasticity (Romano et al., 2014). Subsequently, the reversibility of the phenotype was also confirmed by a study in mice in which the expression of human TDP-43 ΔNLS resulted in the formation of TDP-43 aggregates in the brain and spinal cord, with the concomitant loss of nuclear mouse TDP-43 (Walker et al., 2015). The phenotype could be reversed by halting the expression of human TDP-43 ΔNLS, which in turn was associated with a reduction in TDP-43 aggregation.

Notwithstanding the knowledge acquired about TDP-43 proteinopathies, no treatment is currently available for the human disease that significantly blocks disease progression. Protein aggregation aside, therapeutic approaches have been mainly aimed at targeting one or more of the cellular mechanisms involved in the disease. However, riluzole (Bensimon et al., 1994; Miller et al., 2012), a presynaptic glutamate release inhibitor, and edaravone an antioxidant (Rothstein, 2017), which are the only prescribed treatment options for ALS patients, offer modest survival benefits.

Irrespective of the role played by the aggregates, their reduction represents an important therapeutic pathway worth exploring as their removal might suppress the toxicity of the aggregates or eradicate the aggregates in the cytosol that act as a "sink" sequestering the soluble functional TDP-43 (Cascella et al., 2016). Indeed, removing the cause of the nuclear depletion would then allow TDP-43 to carry out its functions in the nucleus as well as in the cytoplasm. Consequently, strategies that reverse TDP-43 misfolding and restore the native form of the protein have become an emerging target for drug discovery in TDP-43 proteinopathies (De Conti et al., 2017). For example, studies have been undertaken to identify small molecules that stimulate autophagy (Barmada et al., 2014), and for potentiated variants of the protein disaggregase Hsp104 (Torrente et al., 2016). A study was also conducted to identify compounds that reduce TDP-43 aggregation in PC12 cells overexpressing human TDP-43 tagged with GFP that aggregate after oxidative stress (Boyd et al., 2014). Another study screened 1200-FDA approved compound library in a *Drosophila* model that demonstrates lethality due to TDP-43 overexpression (Joardar et al., 2015). In general, the models and screens used to date rely on the overexpression of functional TDP-43 in order to create the aggregates. This is not optimal because of the intrinsic toxicity associated with the high levels of TDP-43, and even more pertinent, because of the many molecular activities regulated by TDP-43, including its self-regulation. A further disadvantage of the screening performed to date, is that they have been mostly directed at specific pathways, thus restricting the scope of the screenings.

In this study, we aimed to build on our previous work to develop and characterise a cellular model of endogenous TDP-43 sequestration by expressing a non-functional mutant TDP-43 that aggregates and sequesters the endogenous protein (Budini et al., 2015). We demonstrate that our cellular model results in efficient aggregation of endogenous TDP-43 and concomitant loss of a known TDP-43 dependent alternative

splicing event regulated by endogenous TDP-43. We demonstrate a proof-of-principle with this model for its use in a high throughput phenotypic screening for the identification of small molecules that can activate any pathway that leads to the enhancement of TDP-43 aggregate clearance. Finally, a validation of the cellular model is provided by recovering the TDP-43 functionality by enhancing aggregate clearance by treating the cells with five different tricyclic compounds. To extend the model to a multicellular organism we constructed a *Drosophila* transgenic strain using the same principles as that in the cellular model in order to test the translational potential of the cellular model, and validate new future therapeutic compounds in vivo. Using these models, we show that thioridazine clears the aggregates through an autophagy-independent mechanism and restore splicing functionality in the cells and locomotion functionality in the *Drosophila* ALS-like model.

2. Materials and methods

2.1. Expression plasmids

The pcDNA5/FRT/TO-EGFP-TDPF4L-12XQ/N expression plasmid for use in the HEK293 Flp—In™ T-Rex™ system (Invitrogen R78007) was created by modifying the pCDNA5/FRT/TO-FLAG-TDPF4L expression plasmid (Budini et al., 2015). The FLAG tag was deleted and simultaneously an *Eco*RV enzyme restriction site was inserted by Quick Change mutagenesis strategy (Stratagene), according to the manufacturer's instructions, using the following oligonucleotides: F4L/pcDNA5 FLAGdel-EcoRVins Forward 5′-atccagcctccggactctagcgtttaaatttaaatcgttaagatatcctttctgaatatattcgggtaaccgaagatgaga-3′ and F4L/pcDNA5 FLAG del-EcoRVins reverse 5′-tctcatcttcggttacccgaatatattcagaaaggatatcttaacg atttaaatttaaacgctagagtccggaggctggat-3′. The EGFP tag was amplified from pEGFP-C2 plasmid using primers carrying an EcoRV target sequence (EcoRV EGFP forward 5′-ccggatatcatggtgagcaagggcga-3′ and EcoRV EGFP reverse 5′-ccggatatcgatctgagtccggccggactt-3′) and cloned into the EcoRV site to generate the pcDNA5/FRT/TO-EGFP-TDPF4L plasmid. Twelve repetitions of the Q/N -rich region of TDP-43 (331–369) were inserted as previously described (Budini et al., 2015). All the cloning steps were followed by sequencing which confirmed all the inserted fragments were correct.

The plasmid pcDNA5ATG/FRT/TO-EGFP-TDPF4L-12XQ/N used to transfect the SHSY-5Y T-Rex cell line, was created by modifying the pcDNA5/FRT/TO-EGFP-TDPF4L-12XQ/N expression plasmid by introducing an ATG codon Additionally, an *Age*I site immediately upstream of the hygromycin resistance gene was added in order to bypass the need for Flip-In system. This was performed by Quick Change mutagenesis strategy (Stratagene) according to the manufacturer's instructions using the following primers forward 5′-agtataggaacttccttggccaccggtttagctatg aaaaagcctgaactcaccgcg-3′ and reverse: 5′-cgcggtgagttcaggctttttcatagct aaaccggtggccaaggaagttcctatact-3′. Subsequently, a CMV promoter, amplified from a pcDNA3 plasmid using the following primers with AgeI site at the extremities F forward: 5′-tatataaccggtcgatgtacgggccagatatac-3'and reverse: 5′-tatataaccggtaatttcgataagccagtaagc-3′, was inserted into the AgeI restriction site to ensure hygromycin expression.

2.2. Cell lines

The HEK293 EGFP-TDPF4L-12XQ/N cell line was created by transfecting the HEK293 Flp—In™ T-Rex™ cell line (Invitrogen R78007) with the pcDNA5/FRT/TO-EGFP-TDPF4L-12XQ/N expression plasmid according to the manufacturer's instructions. Cells were cultured in Dulbecco's modified eagle medium (DMEM) with GlutaMAX (Gibco) supplemented with 10% (*v*/v) heat-inactivated fetal bovine serum (FBS) (Gibco) and antibiotic-antimycotic (Sigma A5955). Hygromycin B (100 μg/mL; (Invitrogen 10687–010) was used to select the stably integrated transgene, and 15 μg/mL blasticidin S (Sigma 15205) was used to maintain selection of the tetracycline repressor (pcDNA6/TR) positive cells. For the induction of the transgene 1 μg/mL of anhydrotetracycline hydrochloride (Sigma 13803–65-1) was added to the culture media for 24 h.

The SHSY-5Y stable cell line expressing EGFP-TDPF4L-12XQ/N was created from SHSY-5Y cell line carrying the stably integrated T-Rex plasmid, which was a kind gift from Christopher Shaw lab (Scotter et al., 2014). Transfection of 2.5 μg of the plasmid pcDNA5ATG/FRT/TO-EGFP-TDPF4L-12XQ/N was performed using Lipofectamine 2000 (Invitrogen P/N 52887), according to the manufacturer's instructions. Cells were cultured in DMEM with GlutaMAX (Gibco) supplemented with 10% (*v*/v) FBS (Gibco) and antibiotic-antimycotic (Sigma A5955). Monoclones containing the transgene of interest together with the tetracycline repressor gene were selected using 150 μg/mL of hygromycin B (Invitrogen 10687–010) and 5 μg/mL of blasticidin S (Sigma 15205). To induce the transgenic protein 60 ng/mL of anhydrotetracycline hydrochloride (Sigma 13803–65-1) was added to the culture media.

2.3. Compound solutions

All the compounds were purchased from Sigma-Aldrich: nortriptyline hydrochloride (N7261), chlorpromazine hydrochloride (C8138), fluphenazine dihydrochloride (F4765), thioridazine hydrochloride (T9025), and clomipramine hydrochloride (C7291).

Stock solutions were prepared in dimethyl sulfoxide (DMSO) at 10 mM, and were serially diluted in DMEM with GlutaMAX (Gibco) supplemented with 10% (v/v) FBS (Gibco) immediately before use. DMSO solutions were used in the control experiments and was prepared following the same procedure as with the compounds. Compounds used to feed the fly larvae were suspended in 1.2 mL of 100% ethanol, vortexed, and incubated at 48 °C for 3–5 min. The resultant compound was added to 120 mL of liquid fly food, at 40 °C fly food (final percentage of ethanol in the food was 1%). For the feeding of adult flies, the compounds were suspended in 100% ethanol (7.5 mL), vortexed and incubated at 48 °C for 3–5 min. The resultant compound was then added to 142.5 mL of the food (the final percentage of ethanol in the food was 5%). The mixture was subsequently aliquoted into individual tubes and allowed to solidify.

2.4. Clearance assay

A total of 100,000 HEK293 cells/well or 70,000 SHSY-5Y cells/well were seeded in a 6-wells plate and immediately induced using anhydrotetracycline hydrochloride for 24 h. In the control group an equivalent amount of water was added to the medium instead of anhydrotetracycline hydrochloride. After 24 h, $t = 0$ cells (cells treated with anhydrotetracycline hydrochloride and uninduced cells) were harvested. Cells to be tested with test compounds were washed twice with 2 mL 1×phosphate buffered saline (PBS), and fresh culture medium without antibiotic-antimycotic was added together with the test compound. An equivalent amount of DMSO was added to control cells. After 48 h, in the case of the HEK293 cells and 72 h in the case of SHSY-5Y cells, the cells were washed with 2 mL of 1× PBS and harvested to extract the protein and RNA.

2.5. Immunoblotting

Proteins were extracted from cells by harvesting them in lysis buffer (15 mM HEPES pH 7.5, 250 mM NaCl, 0.5% (*v*/v) NP-40, 10% (v/v) glycerol and protease inhibitors [Roche Diagnostic 11836170001]), followed by sonication for 10 min at the highest potency. The total cell lysate (without centrifugation) was quantified by the Bradford assay using Biorad reagent (Biorad 500–0006). and 20–30 μg of protein extract was loaded and separated by 10 or 12,5% SDS-PAGE, followed by transfer to nitrocellulose membranes (Whatman NBA083C) and probed with the following primary antibodies: rabbit anti-GFP (1:1000, Santa Cruz sc-8334), rabbit anti-TDP-43 (1:1000, Proteintech 10782–2-

AP), rabbit anti-LC3B (1:1000, Sigma L7543), guinea pig anti-p62 (1:1000, Progen GP62-C), mouse anti-Flag (1:1000, Sigma F1804), rabbit anti-TBPH (1:1500 home-made), mouse anti-tubulin (1:4000, Calbiochem CP06) and rabbit anti-GAPDH (1:1000, Santa Cruz sc-25778). The membranes were incubated with the following secondary antibodies: HRP-labelled anti-mouse (1:2000, Thermo Scientific 32430), HRP-labelled anti-guinea pig (1:10000, Jackson ImmunoResearch 706–035-148) or HRP-labelled anti-rabbit (1:2000, Thermo Scientific 32460). Protein detection was performed using ECL western blotting substrate (Thermo Scientific 32106). ImageJ software was used to quantify intensity of protein signals. Unpaired *t*-test analysis was used to compare the measurements between the 2 groups in different conditions as described in the manuscript. The intensity of the band of interest was normalised to that of tubulin or GAPDH. Values are derived from at least three independent experiments. The significance between the variables was shown based on the *p*-value obtained.

2.6. Splicing assay

Cells with and without drug treatment were harvested and RNA was extracted using EUROGOLD TriFast reagent (Euroclone EMR507100), according to the manufacturer's instructions. After retrotranscription with M-MLV reverse transcriptase (Invitrogen M1701), total cDNA was analysed by polymerase chain reaction (PCR) using the primers: POLDIP3 forward (5′-gcttaatgccagaccgggagttgga-3′) and POLDIP3 reverse (5′-tcatcttcatccaggtcatataaatt-3′) or MADD exon 30 forward: 5′-gacctgaattgggtggcgagttccct-3′ and MADD exon 32 reverse (5′-cattggtgtcttgtacttgtggctc-3′). PCR was performed using DNA polymerase (Biolabs M0273L). All PCR products were analysed on 2% (*w/v*) agarose gels and stained with ethidium bromide (Sigma E1510).

ImageJ software was used to quantify percentage of each isoform upon exposure of the cells to different treatments, as described throughout the manuscript. Unpaired t-test analysis was used to compare the measurements between the 2 groups. The significance between the variables was shown based on the p-value obtained. Values are presented as the mean of three independent experiments.

2.7. RNA interference

Depletion of endogenous TDP-43 from the HEK293 EGFP-TDPF4L-12XQ/N cell line was achieved by RNA interference using HiPerFect Transfection Reagent (Qiagen) and a specific siRNA targeting TDP-43 mRNA (Sigma; target sequence 5′-gcaaagccaagaugagccu-3′) as previously described (De Conti et al., 2015).

2.8. High Throughput live cell imaging TDP-43 Aggregate Clearance Assay

HEK293-EGFP-TDPF4L-12XQ/N cells (3 million) were seeded in a T175 flask and left to grow for 72 h under selection and then induced using anhydrotetracycline hydrochloride for a further 24 h. After induction, cells were washed twice with 1× PBS and seeded in fresh culture medium without antibiotic-antimycotic in poly D-lysine-coated black clear 384-well plates (Greiner Bio-One), using a Viaflo 384 liquid dispenser (Integra). Uninduced HEK293-EGFP-TDPF4L12XQ/N cells were used as controls on each plate. The seeding density was 900 cells/well in 38 μL. Cells were allowed to adhere and grow for 24 h at 37 °C, and 5% CO_2. Compound addition was performed using a Biomek FX liquid dispenser, and 10-point half-log dilutions with a top concentration of 10 μM were prepared in 384-well V-bottom plates (Greiner Bio-One). The compounds were diluted 1:25 into intermediate dilution plates containing 24 μL DMEM-10% FCS and then diluted 1:13.3 into the cell plates. The cells were returned to the incubator for 48 h. Regarding dye addition and imaging: Hoechst 33342 (16.2 mM stock solution in water; Thermo Fisher Scientific) was diluted 1:500 in DMEM-10%FCS medium. Using a Biomek FX liquid dispenser, 2 μL of the dye solution was added to the cell plates. Plates were placed in a Cytomat 6001 carousel incubator (Thermo Scientific) for 1-7 h prior to batch imaging on an IN Cell 2000 Analyser high content imager (GE Healthcare) using a 10× objective. Exposure was set at 100 ms for 4′,6-diamidino-2-phenylindole (DAPI), 700 ms for fluorescin isothiocyanate (FITC), and 700 ms for Texas Red. Automated imaging was achieved using a KiNEDx robot arm and the Overlord software (PAA). Images were analysed using the INCell Developer Toolbox 1.9.2 software (GE Healthcare). Imaging readouts were as follows: total number of aggregates per well (green fluorescent tag; measure of aggregate clearance), total number of cells per well and average nuclear diameter (Hoechst staining; measure of cell viability). Data were normalised to DMSO-treated cells, and dose response curves were fitted using a four-parameter logistic equation with variable slope in Graphpad PRISM 5.

2.9. Autophagy and proteasome inhibition

After EGFP-TDPF4L-12XQ/N induction, anhydrotetracycline was washed out and 1 h before the addition of the test compound, proteasomal or autophagy inhibitors were added to the culture medium. For the autophagy blockage, 30 mM of NH_4Cl (Merck 101145) or 10 μM chloroquine (Sigma C6628) were used. For proteasome inhibition 7 nM bortezomib (Selleckem S1013) was used. After 48 h, the cells were collected and, proteins and RNA were extracted.

2.10. Immunofluorescence

Cells were fixed in 3.7% paraformaldehyde (PFA)/PBS 1× for 15 min at room temperature, permeabilized using 0.3% Triton/PBS 1× for 5 min on ice, and blocked with 2% BSA/PBS 1× for 20 min at room temperature. Immunolabeling using specific antibodies was carried out at room temperature for 1 h in 2% BSA/PBS 1× using rabbit anti-TDP-43 (1:200, Proteintech 10782–2-AP), and the secondary antibody Alexa 594 anti-rabbit (1:500, Invitrogen 997874). For mounting, the slide was placed upside down on a cover slip with a small drop of the mounting medium containing DAPI (Vector Laboratories H1200) to stain the nuclei. The samples were imaged using a confocal laser-scanning microscope (LSM 510 META; Carl Zeiss, Inc.). Images were acquired using 63× or 40× oil immersion objective and processed with ImageJ software.

2.11. TDP-43 solubility assay

A solubility assay using cell lines was performed as previously described (Budini et al., 2015) with minor modifications. Briefly cells were collected, in lysis buffer (15 mM Hepes pH 7.5, 250 mM NaCl, 0.5% (*v*/v) NP-40, 10% (v/v) Glycerol and protease inhibitors [Roche Diagnostic 11836170001]), and sonicated for 10 min at the highest potency. The protein content of the cell lysate was quantified by the Bradford assay using Biorad reagent (Biorad 500–0006). Protein (250 μg) from the cell lysate was ultracentrifuged at 33,000 rpm in a clean Beckman thick-wall centrifuge polycarbonate tube (rotor type 70.1Ti) for 1 h at 25 °C. The supernatant was collected as the soluble fraction and the pellet, as the insoluble fraction was resuspended in urea buffer (7 M urea, 4% CHAPS, 30 mM Tris pH 8,5). To analyse each fraction, 10% of each fraction was loaded to an SDS-PAGE gel followed by western blotting.

The solubility assay for the *Drosophila* models was performed as previously described (Cragnaz et al., 2014).

2.12. Drosophila models

TDPF4L-12XQ/N sequence (Budini et al., 2015) linked to a FLAG tag under the control of an upstream activating sequence (UAS) was cloned in a pUASTattb vector (Bischof et al., 2007) as well as the EGFP construct. The constructs were sequenced and subsequently used to

create transgenic flies using standard embryo injections (Best Gene Inc.). A specific insertion using strain 24486 was chosen for FLAG-TDPF4L-12XQ/N. All transgenic flies were subsequently balanced on the required chromosome. *Drosophila* stocks GMR-Gal4 and ELAV-Gal4 were obtained from the Bloomington *Drosophila* Stock Centre at Indiana University (http://flystocks.bio.indiana.edu/). EGFP files were created as previously described (Cragnaz et al., 2014).

2.13. Larval movement

Wandering third-instar larvae were selected, gently washed and transferred to a petri dish (0.7% agarose in distilled water). After a period of adaptation (30 s), the peristaltic waves within a 2-min period were counted. At least 20 larvae were assayed for each genotype. Unpaired *t*-test analysis was used to compare the measurements between the two groups.

2.14. Climbing assay

Age-synchronized cohorts of flies were transferred without anaesthesia to a 50-mL glass cylinder and tapped to the bottom with cotton. After a period of adaptation of 30 s, the climbing ability of the flies was quantified as the number of flies that reached the top of the cylinder (10 cm) in 15 s. Flies were assayed in batches of 20 (male:female ratio 1:1), and the test was repeated three times for each batch of animals.

In the climbing assay after compound feeding, crosses were set directly in the tubes containing food with or without the compound. After 5 days, the males and females were discarded. One-day-old flies were collected over a period of 2 days and placed in tubes with the test compound or equivalent amount of ethanol in which the test compound was dissolved, in a male:female ratio of 1:1 ratio. The food was changed every second day and after 10 days the climbing ability of the flies was tested.

At least 120 flies were tested under each condition. Statistical analysis was performed using an by unpaired t-test.

2.15. Immunoblotting of fly head samples

The total protein was extracted from the fly head. Whole flies were frozen in liquid nitrogen and then vortexed to separate their heads from the body. *Drosophila* heads were homogenised in lysis buffer (10 μL/head) (10 mM Tris-HCl, pH 7,4, 150 mM NaCl, 5 mM EDTA, 5 mM EGTA, 10% (*v*/v) glycerol, 50 mM NaF, 5 mM DTT, 4 M urea, and protease inhibitors [Roche Diagnostic 11836170001]). After homogenisation, samples were left on ice for 20 min followed by centrifugation at 2,000 rmp for 7 min at 4 °C. Supernatants were collected, used and/or stored at −80 °C.

Proteins were separated by 8% SDS-PAGE, transferred to nitrocellulose membranes (Whatman NBA083C) and probed with the following primary antibodies: mouse anti-FLAG (1:1,000, Sigma F1804), mouse anti-GFP (1:1000, Roche 11814460001), rabbit anti-TBPH (1:1,500, homemade), mouse anti-SYX 8C3s (1:2500, Developmental Studies Hybridoma Bank, DSHB, Iowa City, IA, USA) and mouse anti-tubulin (1:4,000, Calbiochem CP06). The membranes were incubated with the following secondary antibodies: HRP-labelled anti-mouse (1:2000, Thermo Scientific 32430) or HRP-labelled anti-rabbit (1:2000, Thermo Scientific 32460). Finally, protein detection was assessed using a Femto Super Signal substrate (Thermo Scientific 34095). Protein bands were quantified using the NIH ImageJ software. The intensity of the band of interest was normalised to that of tubulin.

3. Results

3.1. Development of a TDP-43 aggregation cellular model for compound screening

A construct, EGFP-TDPF4L-12XQ/N, was created, and Flp-In T-REx recombinant human embryonic kidney cells (HEK293) were used to generate a cell line that stably expresses a single copy of the transgene, under gene expression regulation by tetracycline. As shown in the diagram in Fig. 1A, the construct was composed of EGFP-tagged TDP-43 coding sequence with the mutations F147/149 L and F229/231 L, respectively in the RNA-recognition motifs RRM1 and RRM2, so that the protein was biologically inactive, at least as far as splicing was concerned (D'Ambrogio et al., 2009). It was linked to 12 repetitions of an aggregation-prone region of TDP-43, rich in asparagine and glutamine residues (c.331–369), termed 12XQ/N, which we have previously shown to cause TDP-43 self-aggregation (Budini et al., 2012).

As expected, immunofluorescence analyses showed, that prior to tetracycline induction of the transgene, endogenous TDP-43 is mainly a homogenously distributed nuclear protein (Fig. 1B III). Upon induction of the transgene, through the addition of tetracycline, the expression of EGFP-TDPF4L-12XQ/N triggered the formation of aggregates (Fig. 1B VI), which sequestered endogenous TDP-43 (Fig. 1B VII and VIII). Western blot analysis of the soluble and insoluble protein fraction from the EGFP-TDPF4L-12XQ/N cell line, with and without tetracycline induction substantiates the immunofluorescence analyses, showing that the EGFP-TDPF4L-12XQ/N protein was present almost exclusively in the insoluble fraction (Fig. 1C lane 3 vs. lane 4), as well as a clear shift in the solubility of endogenous TDP-43, upon EGFP-TDPF4L-12XQ/N expression (Fig. 1C lane 2 vs. lane 4).

A reduction in soluble TDP-43, due to its inclusion in the aggregates, should produce a concomitant loss of the endogenous TDP-43 cellular splicing function, we analysed the pattern of *POLDIP3* exon 3 splicing. Inclusion of this exon has been shown to be dependent on TDP-43, as mentioned in the introduction (Fiesel et al., 2012; Shiga et al., 2012). Formation of EGFP-TDPF4L-12XQ/N aggregates and sequestration of endogenous TDP-43 (Fig. 1B) with the consequent reduction of soluble endogenous TDP-43 levels (Fig. 1C) generates a shift in the *POLDIP3* exon 3 splicing pattern (Fig. 1D lane 3 vs. lane 4) analogous to that observed when TDP-43 was silenced (Fig. 1D lane 1 vs. lane 2).

Curiously, the splicing shifts due to the sequestration of TDP-43 in the aggregates and knockdown were identical, notwithstanding that a significant proportion of TDP-43 was still visible in the soluble fraction upon aggregate sequestration of the protein (Fig. 1 C lane 3). However, this is in line with a previous observation that the switch between the two isoforms occurs with a reduction and not a total absence of TDP-43 levels (Fiesel et al., 2012). A further factor contributing to the switch between the TDP-43 dependent *POLDIP3* exon 3 isoforms, notwithstanding the amount of TDP-43 in the soluble fraction, could be that part of the soluble fraction may also be composed of misfolded or oligomerized TDP-43, which occur in initial steps of the aggregation process and are not yet insoluble (French et al., 2019; Jiang et al., 2017).

3.2. EGFP-TDPF4L-12XQ/N expressing cell line can be a tool for screening of compounds for the capacity to clear the EGFP-TDPF4L-12XQ/N aggregates and restore TDP-43 functionality

The characteristics of the cell line described above, including endogenous TDP-43 aggregation that results in a decrease in the soluble TDP-43 with a concomitant loss of TDP-43 splicing function, together with a fluorescent tag allowing for live imaging, provide a unique model for conducting a high-throughput phenotypic screening for compounds

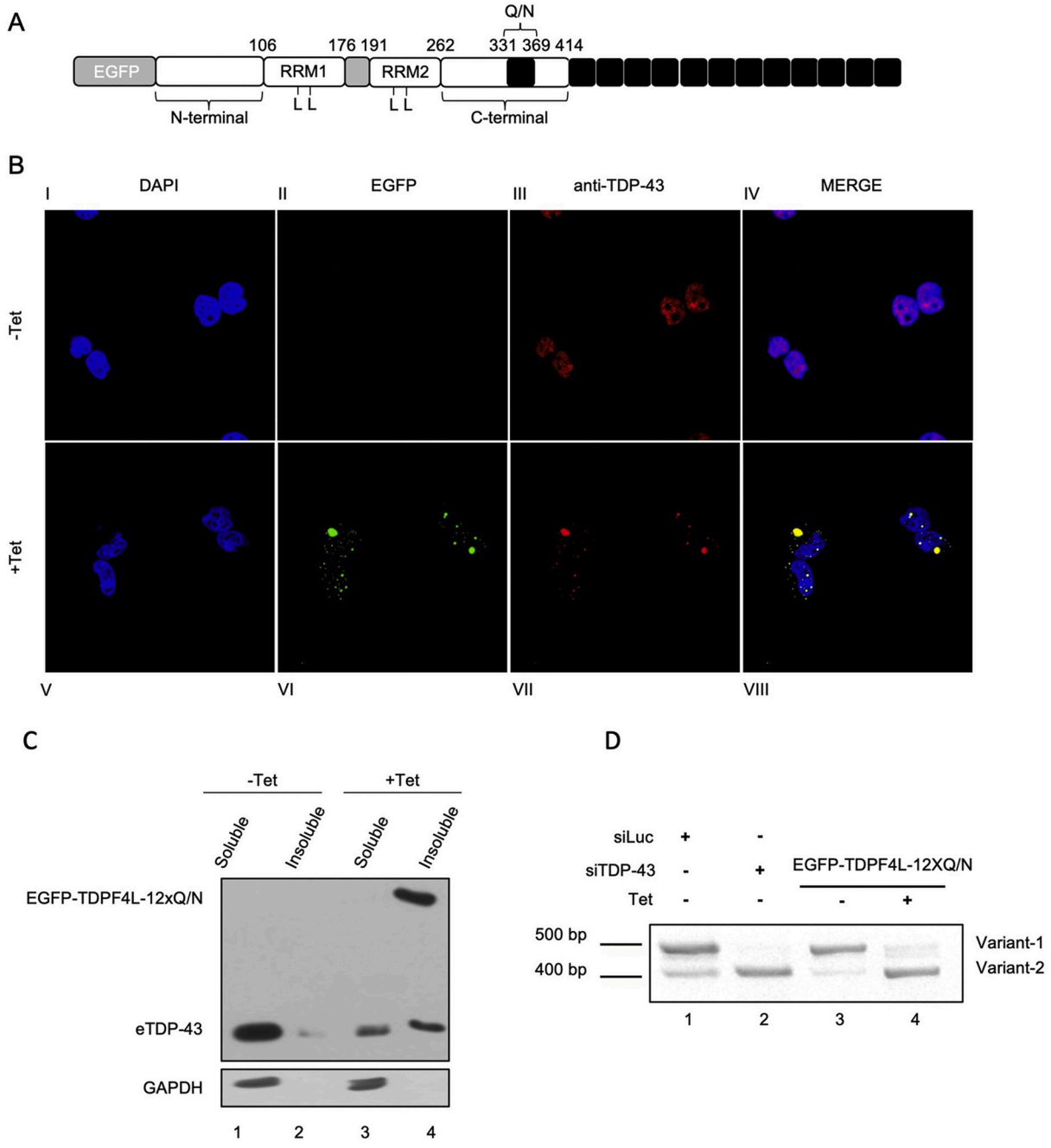

Fig. 1. EGFP-TDPF4L 12XQ/N expression causes aggregation and sequestration of endogenous TDP-43 which results in a loss of splicing of a TDP-43 dependent splicing target. (A) Schematic representation of the EGFP-TDPF4L-12XQ/N construct used for the creation of the aggregation cellular model. Mutations of the leucine residues in the RRM 1 and 2 domains at positions 147, 149, 229, 231 into phenylalanine are represented by L. Black square indicates the Q/N-rich region (region from amino acid 331 to 369) added as 12 repetitions at the end of the TDP-43 sequence. (B) Immunofluorescence of the HEK293 EGFP-TDPF4L-12XQ/N cell line. Upper panel shows the cells without induction of the transgene by anhydrotetracycline (−tet), and lower panel with induction of the transgene by addition of anhydrotetracycline (+tet). EGFP tagged transgene is shown in green. Anti-TDP-43 antibody localized the protein is shown in red. The cell nuclei are stained with the reagent DAPI (blue). (C) Western blot of soluble and insoluble fractions from EGFP-TDPF4L-12XQ/N stable cells induced or not induced with anhydrotetracycline. EGFP-TDPF4L-12XQ/N and endogenous TDP-43 (eTDP-43) proteins were detected with anti-TDP-43 antibodies and anti-GAPDH (D) RT-PCR results showing the alternative splicing pattern of *POLDIP3* exon 3, upon TDP-43 knockdown, and upon induction of the transgene. Variant-1 indicates the exon 3 containing *POLDIP3* mature transcript, while Variant-2 indicates the exon 3-missing transcript. (For interpretation of the references to colour in this figure legend, the reader is referred to the web version of this article.)

that enhance EGFP-TDPF4L-12XQ/N TDP-43 aggregate clearance and restore TDP-43 functionality with regard to splicing.

As a proof-of-principle, for such a study we analysed the effects of five FDA-approved tricyclic compounds. This class of compounds were chosen because it has been shown to be neuroprotective (Stavrovskaya et al., 2004), and to be able to cross the blood-brain-barrier (Pilkington et al., 2006). Furthermore, although there is contradictory evidence, tricyclic compounds seem to stimulate autophagy (Ashoor et al., 2013; Barmada et al., 2014; Rossi et al., 2009; Tsvetkov et al., 2010).

The clearance assay performed here and in the subsequent analysis was carried out by inducing expression of EGFP-TDPF4L-12XQ/N in the cells by the addition of tetracycline for 24 h. At this time point, induced

and un-induced cells were harvested as reference starting points for both protein and splicing analyses ($t = 0$). Subsequently, expression of the transgene was switched off by removal of tetracycline from the media and 10 μM of the test compound or compound equivalent amount of DMSO alone was added to the media for 48 h ($t = 48$). Upon suspension of tetracycline induction, the cells carry out a natural reduction of the aggregates by the physiological pathways of proteolysis and the cell division process. It follows that we can only measure the ability of a given compound to stimulate the clearance of the EGFP-TDPF4L-12XQ/N aggregates formed by the transgene product, over and above the physiological clearance.

As an initial experiment, we analysed EGFP-TDPF4L-12XQ/N protein levels by western blot analysis after the clearance assay described above. Since most of the EGFP-TDPF4L-12XQ/N protein was in the aggregates (Fig. 1B) and insoluble (Fig. 1C), reduction in the protein levels would suggest clearance of aggregates. The analyses were performed on the total un-centrifuged cell lysates (Fig. 2A). As mentioned above, due to the methodology of the clearance assay, a natural clearance of the protein was observed (Fig. 2A compare at t = 0 with those at t = 48, lanes 2 and 3). However, a significant enhancement of the protein clearance by all the compounds tested was clearly visible (Fig. 2A, lane 4 vs. lane 3, lane 6 vs. lane 5, lane 8 vs. lane 7, lane 10 vs. lane 9, lane 12 vs. lane 11).

As shown in Fig. 1B, C, and D, the aggregates entrap endogenous TDP-43, resulting in a reduction in the soluble TDP-43level and loss of splicing function. Therefore, we analysed the functional consequences of the increased clearance of EGFP-TDPF4L-12XQ/N, by the tricyclic compounds, by analysing the splicing pattern of *POLDIP3* exon 3 with and without each compound. In all cases, addition of the compound generated a significant shift in the splicing pattern of *POLDIP3* to that observed in the wild type condition, with inclusion of exon 3 in the mature transcript (Fig. 2A).

To test the cell line in a phenotypic high throughput scenario and to confirm the data obtained above, as well as to quantify the clearance of the aggregates directly, the compounds were tested using a 10-point dose response curve in a high-content imaging assay with readouts measuring the total number of aggregates per well (green fluorescent tag) and total number of cells per well (Hoechst nuclei staining) using an InCell 2000 and Developer image analysis software. Aggregate counts and cell counts were normalised to the counts in DMSO-treated cells and expressed as percentages (Fig. 2B). All the compounds were observed to enhance the clearance of the aggregates, albeit with a variable EC_{50} value or cell toxicity. At a dose of 10 μM, each compound resulted in a decrease in total number of aggregates per well with the residual amount of the aggregates <20% compared to the DMSO control. The exception was nortriptyline where approximately 50% of aggregates were cleared by 10 μM nortriptyline (EC_{50} of ~9.6 μM; table in Fig. 2C). The similarity of the results between live cell imaging of GFP-tagged TDP-43 aggregates, and the western blots following clearance of EGFP-TDPF4L-12XQ/N, corroborated our reasoning that as EGFP-TDPF4L-12XQ/N protein was in the aggregates and insoluble, reduction in the protein levels would suggest clearance of aggregates.

Generation of dose response curve and EC_{50}, reported in Fig. 2C, allows to rank the compounds tested and showed thioridazine to be the most potent compound at clearing TDP-43 aggregates with an EC_{50} of ~3.3 μM, and nortriptyline the weakest with an EC_{50} of ~9.6 μM. Most compounds did not show any significant toxicity towards the cells at all the doses tested (total number of cells per well >80% of DMSO control) except for thioridazine which reduced the cell count by approximately 50% when tested at 10 μM, but not at other doses.

We further validated the experimental model with two compounds that were representative of the general trend observed: nortriptyline and thioridazine. They were chosen because of their differing potencies, the lowest and the highest, respectively, on aggregate clearance. Immunofluorescence images obtained using 10 μM of each compound (Fig. S1A), clearly confirm visually, the readouts obtained from the InCell 2000 and Developer image analysis with regards to EGFP-TDPF4L-12XQ/N aggregate clearance (Fig. 2B). Furthermore, immunofluorescence showed restoration of the endogenous TDP-43 towards a more wildtype pattern after test compound addition (Fig. S1A). Quantification of soluble TDP-43 from a solubility assay (see Methods) also demonstrated an increase in the soluble fraction of the endogenous TDP-43 (Fig. S1B). An additional splicing event under TDP-43 was also analysed: exon 31 of the *MADD* gene, encoding the MAPK-activating protein. This has previously been observed to undergo skipping upon knockdown of TDP-43. Furthermore, inclusion of a cryptic exon derived from the intronic sequence upstream of exon 31 has also been observed upon TDP-43 aggregation (De Conti et al., 2015). Induction of the EGFP-TDPF4L-12XQ/N and consequent inclusion of the endogenous TDP-43 in the EGFP-TDPF4L-12XQ/N aggregates, as shown in in Fig. 1B, leads to a decrease in the soluble TDP-43 which results in a deregulated *MADD* exon 31 splicing pattern (Fig. S2A). As with *POLDIP3* exon 3, addition of either nortriptyline or thioridazine generated a shift in the splicing pattern of *MADD*-pre-mRNA to that observed in the wild-type condition (Fig. S2A).

To investigate if the TDP-43 aggregation cellular model described above, and the effects of the test compounds were cell line independent, we stably inserted the EGFP-TDPF4L-12XQ/N construct into a human neuronal cell line, SHSY-5Y that had an integrated T-Rex plasmid. As can be seen in Fig. S2B, the cell line behaved in an analogous manner to the HEK293-EGFP-TDPF4L-12XQ/N cell line. Upon induction of the transgene by the addition of tetracycline, the expression of EGFP-TDPF4L-12XQ/N triggered the formation of aggregates. This was associated with a clear shift in *POLDIP3* exon 3 exclusion (Fig. S2C). Treatment with either of the two compounds enhanced EGFP-TDPF4L-12XQ/N aggregate clearance (Fig. S2D) and a return towards the wild-type profile of *POLDIP3* exon 3 inclusion (Fig. S2E).

3.3. *Proteasome inhibitors but not autophagy inhibitors block the enhanced aggregate clearance observed with Nortriptyline and Thioridazine*

Autophagy and the ubiquitin–proteasome pathway are responsible for the degradation of most cellular proteins in eukaryotic cells (Nedelsky et al., 2008). To investigate the proteolytic pathway involved in aggregate clearance upon nortriptyline or thioridazine treatment, we initially examined whether the cells exhibited alterations in the autophagic pathway. Due to the toxicity of thioridazine observed in the 10-point dose-response curve, thioridazine was in a dose of 5 μM. The levels of the autophagosome marker microtubule-associated protein 1 light chain (LC3) (Yoshii and Mizushima, 2017) were measured, and it was found that both the compounds increased the LC3II levels (Fig. 3A and B). This could be a consequence of either, increased autophagosome formation due to a higher autophagy activity, or reduced turnover of the autophagosomes as a result of the downstream inhibition of autophagy degradation (Klionsky et al., 2009). To establish the mechanism by which the compound treatments increased the conversion of LC3I to LC3II, we measured the levels of p62, a protein that serves as a link between LC3II and the ubiquitinated substrates that need to be degraded. This protein is incorporated into the completed autophagosome and is degraded by autophagy; therefore, it accumulates when the autophagy flux is inhibited (Klionsky et al., 2008). As shown in Fig. 3A, p62 accumulates when the cells are treated with nortriptyline, suggesting that the observed aggregate clearance is occurring via a pathway other than autophagy. In contrast, thioridazine treatment, on the other hand, did not result in increased p62 levels (Fig. 3B).

To further investigate the pathway through which treatment with nortriptyline and thioridazine enhanced clearance, compound treatment was performed in the presence of autophagy or proteasome inhibitors. Western blot analysis of EGFP-TDPF4L-12XQ/N after autophagy inhibition by the addition of ammonium chloride or chloroquine, clearly show that treatment of the cells with either compound is still able to

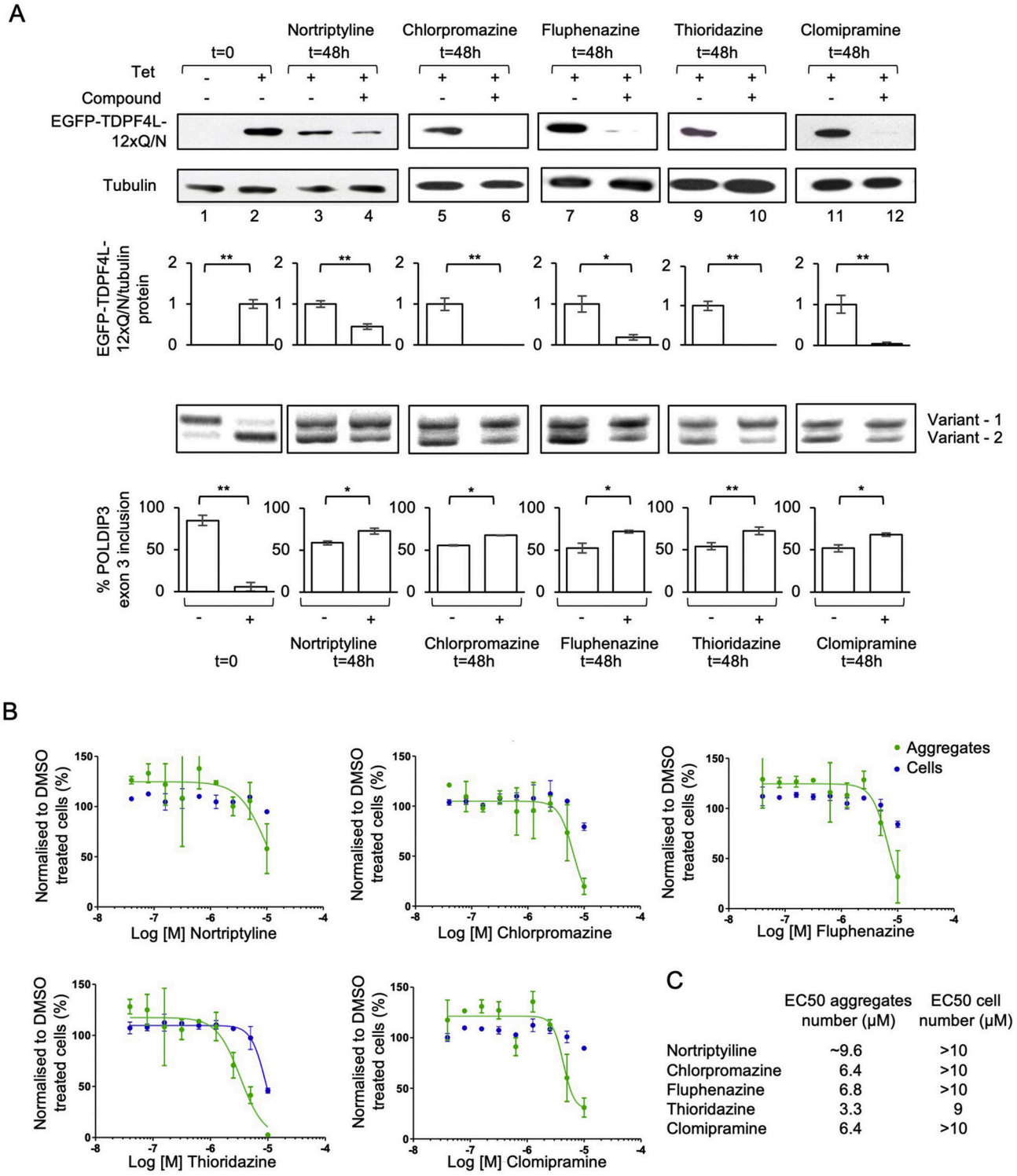

Fig. 2. Tricyclic compounds clear the EGFP-TDPF4L-12XQ/N aggregates and restore TDP-43 splicing function activity. (A) Upper panel: representative western blots using anti-EGFP, which were performed by using total uncentrifuged cell lysates to evaluate the EGFP-TDPF4L-12XQ/ clearance after the treatment with five different tricyclic compounds at a dose of 10 μM. Panel below western blot using anti tubulin. Graphs below shows relative levels of EGFP-TDPF4L-12XQ/N from three independent experiments normalised against tubulin. Lower panel: representative agarose gel following RT-PCR of *POLDIP3* exon 3 splicing pattern from EGFP-TDPF4L-12XQ/N cells prior to and after treatment with the test compounds. Graph below shows quantification for *POLDIP3* exon 3 inclusion from three independent experiments. * indicates $p < 0.05$ and ** indicates $p < 0.01$. Error bars indicate SEM. (B) The 10-point dose response curves for each compound constructed using a high content imaging assay with readouts reported for the total number of aggregates (green) and total number of cells (blue) normalised to the DMSO treated cells (expressed as percentage of DMSO treated cells). Images were taken using an InCell 2000 imager and analysed using Developer software (GE Healthcare) and Graphpad PRISM 5. (C) EC_{50} for each tested compound tested is indicated. (For interpretation of the references to colour in this figure legend, the reader is referred to the web version of this article.)

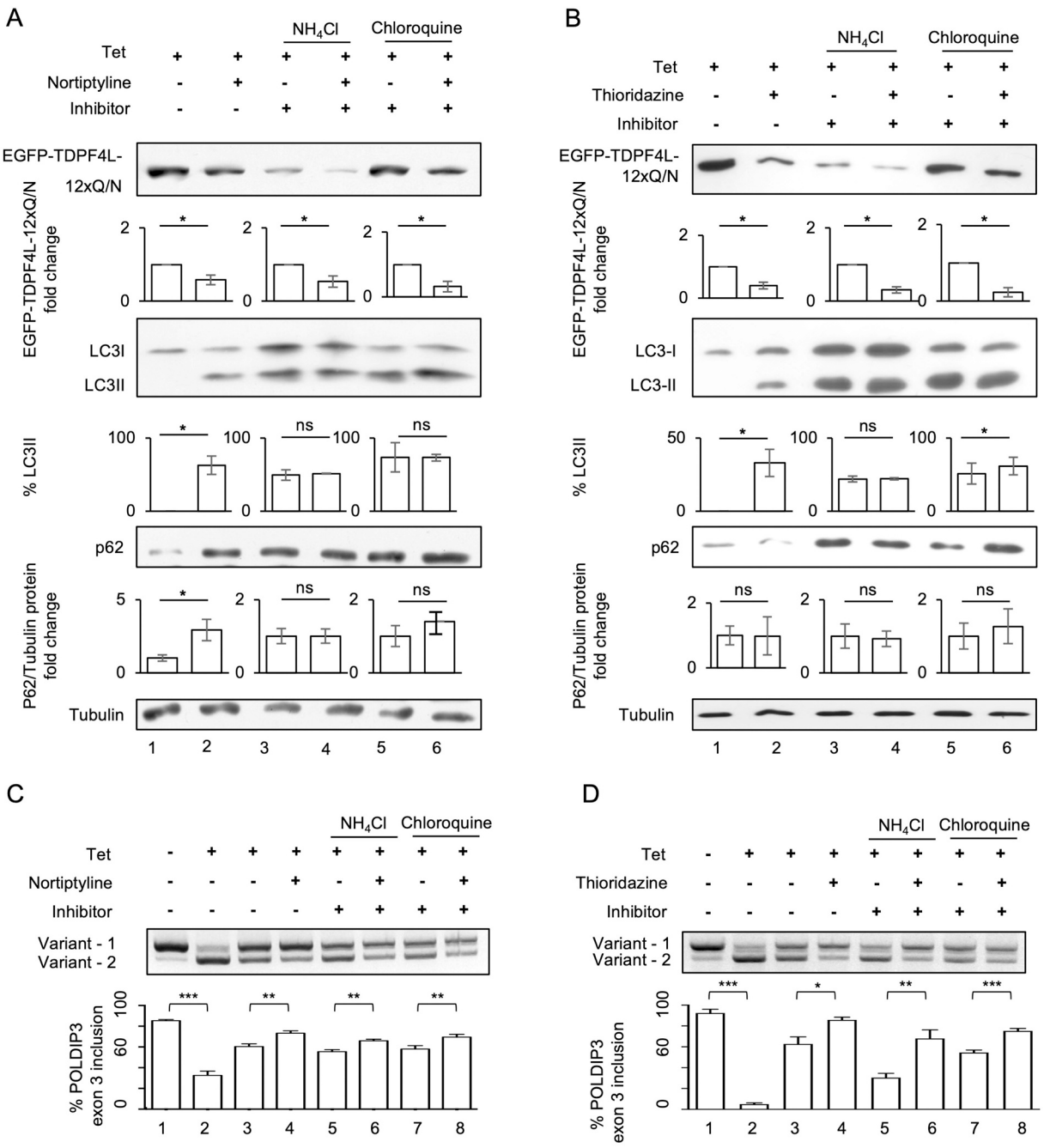

Fig. 3. Autophagy inhibition, does not block the clearance of EGFP-TDPF4L-12XQ/N and restoration of mRNA splicing upon treatment with nortriptyline or thioridazine. (A) Western blots for EGFP-TDPF4L-12XQ/N, LC3 I/LC3II, and p62 in cells treated with nortriptyline, and in presence of NH_4Cl or chloroquine for 48 h Tubulin was used as the loading control (B) Western blots for EGFP-TDPF4L-12XQ/N, LC3 I/LC3II and p62 levels in cells treated with thioridazine, and in presence of NH_4Cl or chloroquine for 48 h. Tubulin was used as the loading control. Graphs below each western blot show fold change in the case of EGFP-TDPF4L-12XQ/N or p63 and percentage of LC3II (C) and (D) show representative agarose gels after RT-PCR of *POLDIP3* exon 3 splicing following treatment with nortriptyline and thioridazine, respectively, in the absence and presence of autophagy inhibition. Graphs show quantification of the inclusion of *POLDIP3* exon 3. * indicates $p < 0.05$, ** indicates $p < 0.01$ and *** indicates $p < 0.001$. Error bars indicate SEM.

enhance EGFP-TDPF4L-12XQ/N clearance (Fig. 3A and B). The fact that clearance of EGFP-TDPF4L-12XQ/N still occurred, notwithstanding inhibition of autophagy, was further confirmed by the analysis of the *POLDIP3* mRNA isoforms, as recovery of *POLDIP3* mRNA variant-1 was observed upon treatment with either compound (Fig. 3C and D). Conversely, when we analysed EGFP-TDPF4L-12XQ/N clearance upon nortriptyline or thioridazine treatment in the presence of the proteasome inhibitor bortezomib, neither compound enhanced the clearance (Fig. 4A and B). Furthermore, both compounds, in the presence of bortezomib, failed to recover the *POLDIP3* wild-type splicing pattern (Fig. 4C and D). These data point to the critical role of the proteasome and not of the autophagosome in the mechanism of enhancement of aggregate clearance by nortriptyline and thioridazine.

Pan-neuronal expression of the FLAG-TDPF4L-12XQ/N construct in *Drosophila melanogaster* results in an adult locomotive defect.

D. melanogaster transgenic flies expressing either 12 repetitions of the Q/N region or an N-terminal sequence of TDP-43 combined with the 12 repetitions of the Q/N domain have been shown to develop a locomotive

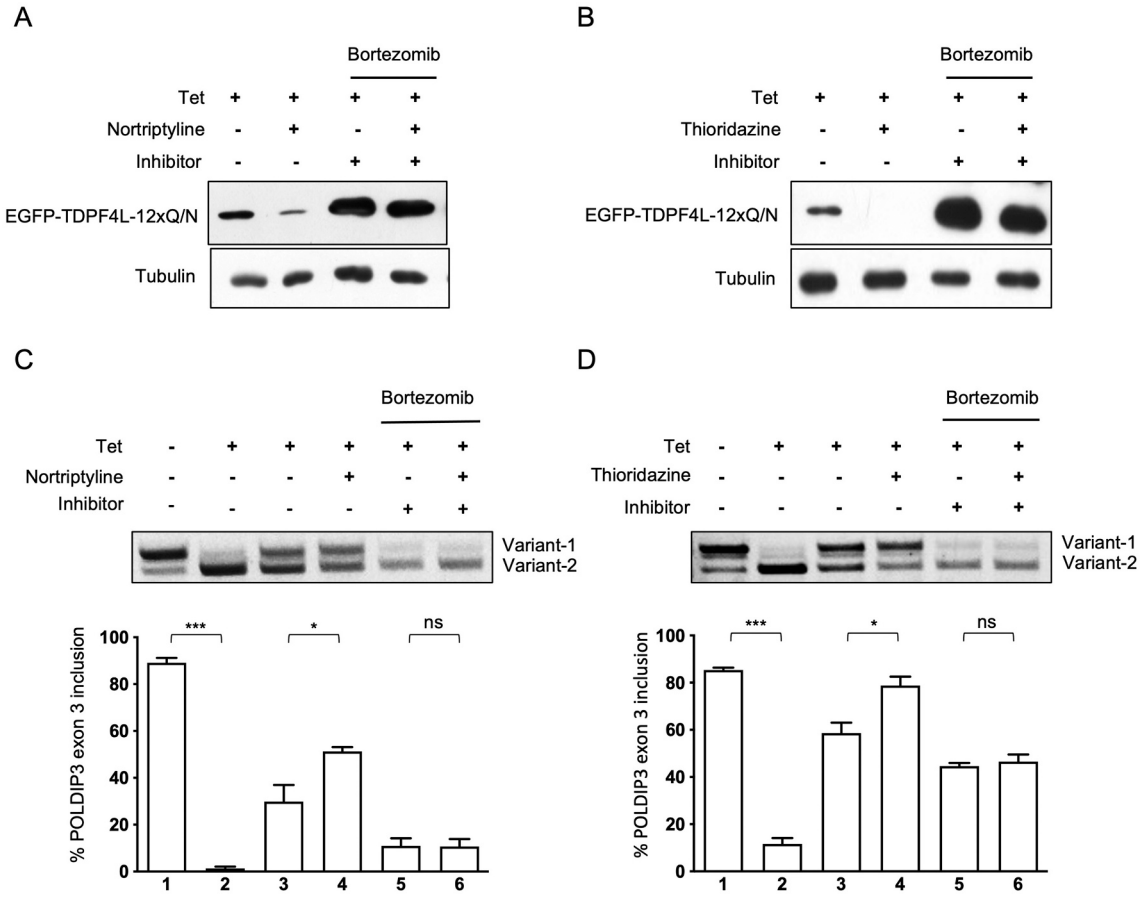

Fig. 4. Proteasome inhibition decreases clearance of EGFP-TDPF4L-12XQ/N aggregate clearance and restoration of mRNA splicing upon nortriptyline or thioridazine treatment. (A) Western blots from a clearance assay showing EGFP-TDPF4L-12XQ/N levels after cells were treated with Nortriptyline in presence of the inhibitor bortezomib. (B) Western blots from clearance assay showing EGFP-TDPF4L-12XQ/N levels after cells were treated with thioridazine in presence of the proteasome inhibitor bortezomib. Tubulin was used as the loading control in both cases. (C) and (D) Show representative agarose gels of RT-PCR of *POLDIP3* exon 3 splicing following treatment with nortriptyline and thioridazine respectively, in presence of the proteasome inhibitor bortezomib. Graphs indicate the quantification of exon 3 inclusion. ns indicates not significant *p* value ($p \geq 0.05$), * indicates $p < 0.05$ and *** indicates $p < 0.001$. Error bars denote SEM.

phenotype. In the case of the former, in adulthood (Cragnaz et al., 2014), and in the case of the latter, in the larval stage (Langellotti et al., 2016).

To study the effects of nortriptyline and thioridazine on TDP-43 aggregation in vivo, we created a transgenic *Drosophila* model expressing a construct that was analogous to that used in the cellular model, described above, with a FLAG-tag instead of GFP. After embryo injection of a FLAG-TDPF4L-12XQ/N transgene under the control of the upstream activating sequence (UAS), five different fly lines were obtained and screened for transgene expression by crossing them with flies carrying the GMR-Gal4 driver (Fig. S3A). Transgenic lines 1 and 5, respectively, under and overexpressed the protein with respect to the other three lines (2, 3, and 4) that expressed the FLAG-TDPF4L-12XQ/N protein at comparable levels. Line 3 was arbitrarily chosen for the rest of the experiments. To show that FLAG-TDPF4L-12XQ/N transgene expression induces the formation of insoluble aggregates capable of trapping endogenous TBPH in flies, we performed biochemical fractionation of proteins extracted from the adult heads of the flies expressing TBPH together with either EGFP or FLAG-TDPF4L-12XQ/N. As shown in Fig. S3B, the FLAG-TDPF4L-12XQ/N protein was present in the insoluble fraction. Moreover, its expression shifts the endogenous TBPH from the soluble to the insoluble fraction, demonstrating the capability of the FLAG-TDPF4L-12XQ/N aggregates to sequester endogenous TBPH, thus rendering it non-functional.

Overexpression of TBPH in the *Drosophila* eye has been shown to result in the degeneration of the external surface of the Drosophila eye. The co-expression of a transgene with 12 repetitions of the Q/N linked to only GFP sequestered the excess TBPH and prevented eye degeneration (Cragnaz et al., 2014). We have also observed that the co-expression of GMR-Gal4 TBPH and our transgene, FLAG-TDPF4L-12XQ/N reverses the degenerative effect of TBPH overexpression (Fig. S3C).

The effects of transgene expression in the neurons on the Drosophila phenotype, were assessed in flies expressing the construct selectively in neurons by crossing the FLAG-TDPF4L-12XQ/N flies with flies containing the pan-neuronal elav-Gal4 driver. The flies with the transgene showed no locomotive phenotype in the larval stage (Fig. 5A). The assessment of the climbing ability of transgenic flies at different time points showed that from day 7, the flies expressing the FLAG-TDPF4L-12XQ/N exhibited a significant decrease in their climbing ability when compared to the control EGFP flies (77% vs. 87%). The severity of the locomotion defect increased with age with less than 10% of the transgenic flies completing the test by arriving at the top of the cylinder at day 14 compared to 85% of the control EGFP flies (Fig. 5B). In an attempt to establish a direct correlation between a biological marker, TDP-43 and the phenotype observed, we analysed the levels of syntaxin protein (SYX also known as Syx1a). Syntaxins are plasma membrane proteins that are implicated in the docking of synaptic vesicles in presynaptic active zones (Wu et al., 1999). Alterations in this protein family have been associated with neurodegenerative diseases (Margiotta, 2021). This presynaptic vesicular protein has been reported to be down regulated in neuromuscular junction and presynaptic boutons in the

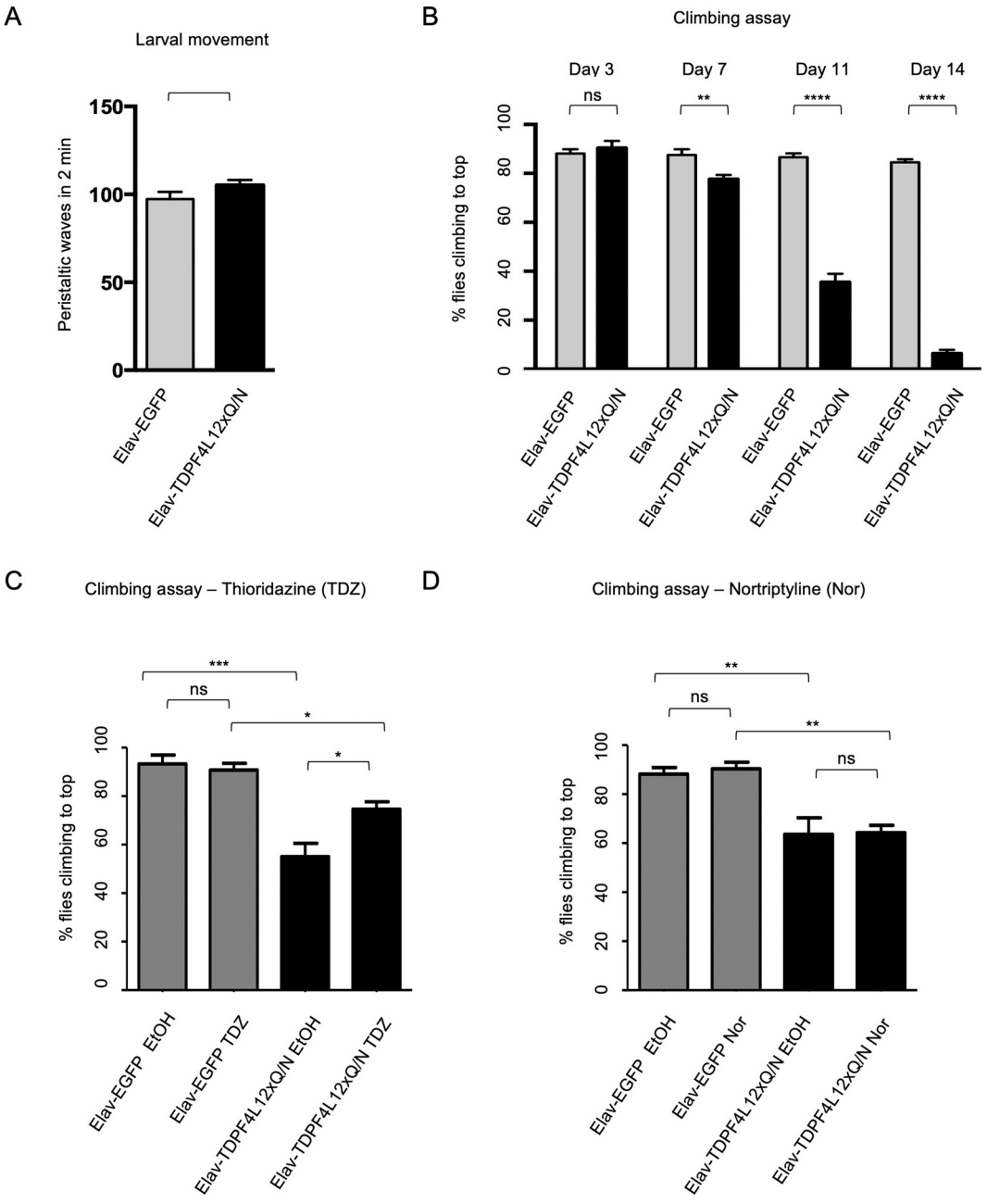

Fig. 5. Adult locomotive defect produced by the pan-neuronal expression of the FLAG-TDPF4L-12XQ/N construct in *Drosophila melanogaster* is rescued by thioridazine.

(A) Quantification of the mean peristaltic waves of third instar larvae, expressing either EGFP (grey) or TDPF4L-12XQ/N (black) under the ELAV-Gal4 driver. More than 20 larvae from each genotype were counted. (B) Analysis of the climbing ability of ELAV-Gal4/UAS-FLAG-TDPF4L-12XQ/N expressing flies (black) compared to that of the ELAV-Gal4/UAS EGFP control flies (grey) at different time points. A total of 100 flies per genotype and time point were used. (C) Climbing ability at the time point of 10 days of the ELAV-Gal4/UAS-FLAG-TDPF4L-12XQ/N expressing flies and EGFP control flies that were treated not-treated with thioradazine. During the larval phase, 50 μM dose was used, while and adult 0.4 mM was used in the adult stage. A total of 100 flies per condition were tested. (D) Climbing ability at 10 days of the ELAV-Gal4/UAS-FLAG-TDPF4L-12XQ/N expressing flies and EGFP control flies treated and non-treated with nortriptyline. During the larval stage 50 μM was used, and 0.4 mM was used in the adult stage. A total of 100 flies per condition were tested. ns indicates not significant p value ($p \geq 0.05$), * indicates $p < 0.05$, ** indicates $p < 0.01$ and *** indicates $p < 0.001$. Error bars denote SEM.

larvae and in the adult heads of TBPH minus flies (Romano et al., 2014), that showed contrary to our model, larvae locomotive phenotypes. We tested two time points, at 3 and 10 days (Fig. S3D), in order to see if we could observe a difference associated with the onset of the locomotive phenotype, which as shown in Fig. 5B is not present at day 3 but significantly so at day 10. However, although we replicated previous results (Fig. S3D compare W118 control vs TBPH minus files) SYX in the FLAG-TDPF4L-12XQ/N vs EGFP flies showed a tendency to decrease, particular so in the time point where the locomotive defect was observed, but this decrease was not statistically significant (Fig. S3D).

To examine whether the positive phenotypic and molecular effects observed in the cellular assays with nortriptyline and thioridazine could translate into a rescue of the motor phenotype observed in the *Drosophila* model, the flies were fed with either compound from the larval stage, and the climbing ability of flies was analysed on day 10. This time point was chosen as we evaluated it to be an optimal compromise between the

appearance of the locomotive defects and its severity. We first identified a higher range of non-toxic dose of thioridazine in the wild type larvae (50 μM) and adult files (0.4 mM). FLAG-TDPF4L-12XQ/N flies fed with the test compound at these concentrations, from larvae through to adult stage, showed a significant improvement in their climbing ability on day 10 compared to non-treated flies (Fig. 5C). In the case of nortriptyline, the flies were fed with the same concentration as thioridazine, which was observed to be non-toxic. However, in this case, no statistically significant improvement was observed (Fig. 5D). It should be noted that in the cellular model nortriptyline was less efficient than thioridazine in aggregate clearance.

4. Discussion

In patients with ALS and FTLD-U, as well as in other TDP-43 proteinopathies, the presence of cytoplasmic TDP-43 aggregates within the affected motor neurons is accompanied by nuclear depletion of this predominantly nuclear protein (Arai et al., 2006; Neumann et al., 2006). Agents that clear this protein aggregation represent a promising therapeutic options either by eliminating toxicity or loss-of-function effects caused by the aggregates or interfere with the formation of the self-templating conformers that catalyse the template-directed replication that occurs with prion-like proteins such as TDP-43 (De Conti et al., 2017), or clear them directly (Furukawa et al., 2011; Nonaka et al., 2013; Smethurst et al., 2016). In this study, we created models for identifying small molecules for this purpose and their analysis in high-throughput phenotypic compound screens.

We created a cellular system expressing an inducible fluorescently tagged TDP-43 aggregate inducer. We demonstrated that aggregate clearance is enhanced upon treatment with tricyclic compounds. Our cellular system can show the effects of the tested compound either phenotypically, by measuring the disappearance of the aggregate's fluorescence, or functionally, by measuring the recovery of the TDP-43 splicing function. This makes the model an invaluable tool for the identification of compounds capable of inducing TDP-43 aggregate clearance, regardless of their mechanism of action.

Interestingly, we observed that the clearance of TDP-43 aggregates upon nortriptyline or thioridazine treatment in our cellular model depends on an active proteasome pathway and is independent of the later stages of autophagy, beyond the fusion step of the nascent autophagosome with the lysosome where the inhibitors exert their mode of action. Previous studies have shown that these compounds are autophagy enhancers (Tsvetkov et al., 2010). On the other hand, in line with our results, there is evidence that tricyclic compounds accumulate in lysosomes and behave as autophagy inhibitors by increasing the pH of the lysosomes, thereby impairing the functioning of lysosomal hydrolases, likely resulting in the inhibition of cargo degradation (Ashoor et al., 2013; Nadanaciva et al., 2011). Regarding the role of the proteasome, it is unlikely that it can directly degrade the aggregates, as proteasome degradation is normally regarded as requiring the complete unfolding of any substrate. However, in a study investigating the role of caspase-cleaved TDP-43 fragments observed in the brain inclusions of ALS patients, a cell model expressing TDP-43C-terminal fragments spanning TDP-43 amino acids 220 to 241 tagged with a GFP label was used and the physiological clearance of the aggregates was also observed to be suppressed by proteasome inhibition, but not by autophagy inhibition (Zhang et al., 2010).

Consistent with the possibility of proteasome degradation of larger aggregates, a recent study showed that the proteasome can clear aggregates through the mammalian proteasome shuttle factor UBQLN2, which acts with the HSP70-HSP110 dis-aggregase machinery system (Hjerpe et al., 2016), and solubilizes the aggregated proteins before accommodating them in the proteasome. In accordance with this new role of UBQLN2, mutations in the *ubiquilin-2* gene have been identified in a fraction of familial ALS cases, in which an impairment of protein degradation has been observed (Deng et al., 2011). Additionally, it is interesting to note that in a study using TDP-43 ΔNLS mice, inclusions could be eliminated with a single-chain variable fragment monoclonal antibody via dual proteasomal and autophagy pathways (Tamaki et al., 2018).

Finally, we showed that the compounds that recovered TDP-43 function in the cellular model also work in vivo. In fact, the FLAG-TDPF4L-12XQ/N *Drosophila* model, created on the same principle as the cell line, displays a locomotion defect in the adult fly. Feeding thioridazine either to the larva or the adult resulted in a significant improvement in their locomotion showing that the results of the in vitro cellular model can be translated to the in vivo *Drosophila* model.

It follows that a high-throughput screening for novel small molecules that are capable of clearing aggregates and recovering TDP-43 functionality in the cellular assay is indicated. In fact, it is likely that such an exercise will produce better in vivo effectors than thioridazine. Furthermore, the use of this cell line model in a high-throughput system will allow the identification of common pathways and key therapeutic targets that can then be manipulated to modulate the disease (Bureau et al., 2017).

In conclusion, we have created a cellular model and established a proof-of-principle for conducting a high-throughput phenotypic screening for the discovery of novel compounds capable of clearing TDP-43 aggregates. We have also shown that therapeutic strategies aimed at re-establishing TDP-43 function may successfully revert the neurological defects associated with TDP-43 aggregation in an animal model. Our observations suggest that a viable therapeutic approach for the treatment of human ALS pathology is to achieve aggregate clearance even in the advance stages of the disease.

Supplementary data to this article can be found online at https://doi.org/10.1016/j.nbd.2021.105515.

Funding

Dementia Consortium Alzheimer's Research UK.

Declaration of Competing Interest

The authors declare no competing interests.

Acknowledgments

The authors thank Alzheimer's Research UK scientific staff in general for useful discussions, particularly Carol Routledge, Sara Imarisio and David Reynolds.

References

Alami, N.H., Smith, R.B., Carrasco, M.A., Williams, L.A., Winborn, C.S., Han, S.S.W., Kiskinis, E., Winborn, B., Freibaum, B.D., Kanagaraj, A., Clare, A.J., Badders, N.M., Bilican, B., Chaum, E., Chandran, S., Shaw, C.E., Eggan, K.C., Maniatis, T., Taylor, J. P., 2014. Axonal transport of TDP-43 mRNA granules is impaired by ALS-causing mutations. Neuron 81, 536–543. https://doi.org/10.1016/j.neuron.2013.12.018.

Arai, T., Hasegawa, M., Akiyama, H., Ikeda, K., Nonaka, T., Mori, H., Mann, D., Tsuchiya, K., Yoshida, M., Hashizume, Y., Oda, T., 2006. TDP-43 is a component of ubiquitin-positive tau-negative inclusions in frontotemporal lobar degeneration and amyotrophic lateral sclerosis. Biochem. Biophys. Res. Commun. 351, 602–611. https://doi.org/10.1016/j.bbrc.2006.10.093.

Ashoor, R., Yafawi, R., Jessen, B., Lu, S., 2013. The contribution of lysosomotropism to autophagy perturbation. PLoS One 8, e82481. https://doi.org/10.1371/journal.pone.0082481.

Ayala, Y.M., Pantano, S., D'Ambrogio, A., Buratti, E., Brindisi, A., Marchetti, C., Romano, M., Baralle, F.E., 2005. Human, Drosophila, and C.elegans TDP43: nucleic acid binding properties and splicing regulatory function. J. Mol. Biol. 348, 575–588. https://doi.org/10.1016/j.jmb.2005.02.038.

Ayala, Y.M., Zago, P., D'Ambrogio, A., Xu, Y.-F., Petrucelli, L., Buratti, E., Baralle, F.E., 2008. Structural determinants of the cellular localization and shuttling of TDP-43. J. Cell Sci. 121, 3778–3785. https://doi.org/10.1242/jcs.038950.

Barmada, S.J., Serio, A., Arjun, A., Bilican, B., Daub, A., Ando, D.M., Tsvetkov, A., Pleiss, M., Li, X., Peisach, D., Shaw, C., Chandran, S., Finkbeiner, S., 2014. Autophagy induction enhances TDP43 turnover and survival in neuronal ALS models. Nat. Chem. Biol. 10, 677–685. https://doi.org/10.1038/nchembio.1563.

Bensimon, G., Lacomblez, L., Meininger, V., 1994. A controlled trial of riluzole in amyotrophic lateral sclerosis. ALS/Riluzole Study Group. N. Engl. J. Med. 330, 585–591. https://doi.org/10.1056/NEJM199403033300901.

Bischof, J., Maeda, R.K., Hediger, M., Karch, F., Basler, K., 2007. An optimized transgenesis system for Drosophila using germ-line-specific phiC31 integrases. Proc. Natl. Acad. Sci. U. S. A. 104, 3312–3317. https://doi.org/10.1073/pnas.0611511104.

Bolognesi, B., Faure, A.J., Seuma, M., Schmiedel, J.M., Tartaglia, G.G., Lehner, B., 2019. The mutational landscape of a prion-like domain. Nat. Commun. 10, 4162. https://doi.org/10.1038/s41467-019-12101-z.

Boyd, J.D., Lee, P., Feiler, M.S., Zauur, N., Liu, M., Concannon, J., Ebata, A., Wolozin, B., Glicksman, M.A., 2014. A high-content screen identifies novel compounds that inhibit stress-induced TDP-43 cellular aggregation and associated cytotoxicity. J. Biomol. Screen. 19, 44–56. https://doi.org/10.1177/1087057113501553.

Budini, M., Buratti, E., Stuani, C., Guarnaccia, C., Romano, V., De Conti, L., Baralle, F.E., 2012. Cellular model of TAR DNA-binding protein 43 (TDP-43) aggregation based on its C-terminal Gln/Asn-rich region. J. Biol. Chem. 287, 7512–7525. https://doi.org/10.1074/jbc.M111.288720.

Budini, M., Romano, V., Quadri, Z., Buratti, E., Baralle, F.E., 2015. TDP-43 loss of cellular function through aggregation requires additional structural determinants beyond its C-terminal Q/N prion-like domain. Hum. Mol. Genet. 24, 9–20. https://doi.org/10.1093/hmg/ddu415.

Buratti, E., Baralle, F.E., 2012. TDP-43: gumming up neurons through protein-protein and protein-RNA interactions. Trends Biochem. Sci. 37, 237–247. https://doi.org/10.1016/j.tibs.2012.03.003.

Bureau, E.A., Mpamhanga, C., Conti, L.D., Wright, P.D., Cragnaz, L., Tickle, D., Kettleborough, C., Baralle, M., Reynolds, D., Brownlees, J., 2017. Phenotypic high-content screen measuring clearance of TDP - 43 aggregates. Alzheimer's & Dementia: J. Alzheimer's Assoc. 13, P292. https://doi.org/10.1016/j.jalz.2017.06.198.

Cascella, R., Capitini, C., Fani, G., Dobson, C.M., Cecchi, C., Chiti, F., 2016. Quantification of the relative contributions of loss-of-function and gain-of-function mechanisms in TAR DNA-binding protein 43 (TDP-43) Proteinopathies. J. Biol. Chem. 291, 19437–19448. https://doi.org/10.1074/jbc.M116.737726.

Cozzolino, M., Carrì, M.T., 2012. Mitochondrial dysfunction in ALS. Prog. Neurobiol. 97, 54–66. https://doi.org/10.1016/j.pneurobio.2011.06.003.

Cragnaz, L., Klima, R., Skoko, N., Budini, M., Feiguin, F., Baralle, F.E., 2014. Aggregate formation prevents dTDP-43 neurotoxicity in the Drosophila melanogaster eye. Neurobiol. Dis. 71, 74–80. https://doi.org/10.1016/j.nbd.2014.07.009.

Cragnaz, L., Klima, R., De Conti, L., Romano, G., Feiguin, F., Buratti, E., Baralle, M., Baralle, F.E., 2015. An age-related reduction of brain TBPH/TDP-43 levels precedes the onset of locomotion defects in a Drosophila ALS model. Neuroscience 311, 415–421. https://doi.org/10.1016/j.neuroscience.2015.10.037.

Dadon-Nachum, M., Melamed, E., Offen, D., 2011. The "dying-back" phenomenon of motor neurons in ALS. J. Mol. Neurosci. 43, 470–477. https://doi.org/10.1007/s12031-010-9467-1.

D'Ambrogio, A., Buratti, E., Stuani, C., Guarnaccia, C., Romano, M., Ayala, Y.M., Baralle, F.E., 2009. Functional mapping of the interaction between TDP-43 and hnRNP A2 in vivo. Nucleic Acids Res. 37, 4116–4126. https://doi.org/10.1093/nar/gkp342.

De Conti, L., Akinyi, M.V., Mendoza-Maldonado, R., Romano, M., Baralle, M., Buratti, E., 2015. TDP-43 affects splicing profiles and isoform production of genes involved in the apoptotic and mitotic cellular pathways. Nucleic Acids Res. 43, 8990–9005. https://doi.org/10.1093/nar/gkv814.

De Conti, L., Borroni, B., Baralle, M., 2017. New routes in frontotemporal dementia drug discovery. Expert Opin. Drug Discovery 12, 659–671. https://doi.org/10.1080/17460441.2017.1329294.

Deng, H.-X., Chen, W., Hong, S.-T., Boycott, K.M., Gorrie, G.H., Siddique, N., Yang, Y., Fecto, F., Shi, Y., Zhai, H., Jiang, H., Hirano, M., Rampersaud, E., Jansen, G.H., Donkervoort, S., Bigio, E.H., Brooks, B.R., Ajroud, K., Sufit, R.L., Haines, J.L., Mugnaini, E., Pericak-Vance, M.A., Siddique, T., 2011. Mutations in UBQLN2 cause dominant X-linked juvenile and adult-onset ALS and ALS/dementia. Nature 477, 211–215. https://doi.org/10.1038/nature10353.

Feiguin, F., Godena, V.K., Romano, G., D'Ambrogio, A., Klima, R., Baralle, F.E., 2009. Depletion of TDP-43 affects Drosophila motoneurons terminal synapsis and locomotive behavior. FEBS Lett. 583, 1586–1592. https://doi.org/10.1016/j.febslet.2009.04.019.

Fiesel, F.C., Weber, S.S., Supper, J., Zell, A., Kahle, P.J., 2012. TDP-43 regulates global translational yield by splicing of exon junction complex component SKAR. Nucleic Acids Res. 40, 2668–2682. https://doi.org/10.1093/nar/gkr1082.

French, R.L., Grese, Z.R., Aligireddy, H., Dhavale, D.D., Reeb, A.N., Kedia, N., Kotzbauer, P.T., Bieschke, J., Ayala, Y.M., 2019. Detection of TAR DNA-binding protein 43 (TDP-43) oligomers as initial intermediate species during aggregate formation. J. Biol. Chem. 294, 6696–6709. https://doi.org/10.1074/jbc.RA118.005889.

Furukawa, Y., Kaneko, K., Watanabe, S., Yamanaka, K., Nukina, N., 2011. A seeding reaction recapitulates intracellular formation of Sarkosyl-insoluble transactivation response element (TAR) DNA-binding protein-43 inclusions. J. Biol. Chem. 286, 18664–18672. https://doi.org/10.1074/jbc.M111.231209.

Geser, F., Martinez-Lage, M., Kwong, L.K., Lee, V.M.-Y., Trojanowski, J.Q., 2009. Amyotrophic lateral sclerosis, frontotemporal dementia and beyond: the TDP-43 diseases. J. Neurol. 256, 1205–1214. https://doi.org/10.1007/s00415-009-5069-7.

Hjerpe, R., Bett, J.S., Keuss, M.J., Solovyova, A., McWilliams, T.G., Johnson, C., Sahu, I., Varghese, J., Wood, N., Wightman, M., Osborne, G., Bates, G.P., Glickman, M.H., Trost, M., Knebel, A., Marchesi, F., Kurz, T., 2016. UBQLN2 mediates autophagy-independent protein aggregate clearance by the proteasome. Cell 166, 935–949. https://doi.org/10.1016/j.cell.2016.07.001.

Iguchi, Y., Katsuno, M., Niwa, J., Takagi, S., Ishigaki, S., Ikenaka, K., Kawai, K., Watanabe, H., Yamanaka, K., Takahashi, R., Misawa, H., Sasaki, S., Tanaka, F., Sobue, G., 2013. Loss of TDP-43 causes age-dependent progressive motor neuron degeneration. Brain 136, 1371–1382. https://doi.org/10.1093/brain/awt029.

Jiang, L.-L., Xue, W., Hong, J.-Y., Zhang, J.-T., Li, M.-J., Yu, S.-N., He, J.-H., Hu, H.-Y., 2017. The N-terminal dimerization is required for TDP-43 splicing activity. Sci. Rep. 7, 6196. https://doi.org/10.1038/s41598-017-06263-3.

Joardar, A., Menzl, J., Podolsky, T.C., Manzo, E., Estes, P.S., Ashford, S., Zarnescu, D.C., 2015. PPAR gamma activation is neuroprotective in a Drosophila model of ALS based on TDP-43. Hum. Mol. Genet. 24, 1741–1754. https://doi.org/10.1093/hmg/ddu587.

Klionsky, D.J., Abeliovich, H., Agostinis, P., Agrawal, D.K., Aliev, G., Askew, D.S., Baba, M., Baehrecke, E.H., Bahr, B.A., Ballabio, A., Bamber, B.A., Bassham, D.C., Bergamini, E., Bi, X., Biard-Piechaczyk, M., Blum, J.S., Bredesen, D.E., Brodsky, J.L., Brumell, J.H., Brunk, U.T., Bursch, W., Camougrand, N., Cebollero, E., Cecconi, F., Chen, Y., Chin, L.-S., Choi, A., Chu, C.T., Chung, J., Clarke, P.G.H., Clark, R.S.B., Clarke, S.G., Clavé, C., Cleveland, J.L., Codogno, P., Colombo, M.I., Coto-Montes, A., Cregg, J.M., Cuervo, A.M., Debnath, J., Demarchi, F., Dennis, P.B., Dennis, P.A., Deretic, V., Devenish, R.J., Di Sano, F., Dice, J.F., Difiglia, M., Dinesh-Kumar, S., Distelhorst, C.W., Djavaheri-Mergny, M., Dorsey, F.C., Dröge, W., Dron, M., Dunn, W.A., Duszenko, M., Eissa, N.T., Elazar, Z., Esclatine, A., Eskelinen, E.-L., Fésüs, L., Finley, K.D., Fuentes, J.M., Fueyo, J., Fujisaki, K., Galliot, B., Gao, F.-B., Gewirtz, D.A., Gibson, S.B., Gohla, A., Goldberg, A.L., Gonzalez, R., González-Estévez, C., Gorski, S., Gottlieb, R.A., Häussinger, D., He, Y.-W., Heidenreich, K., Hill, J.A., Høyer-Hansen, M., Hu, X., Huang, W.-P., Iwasaki, A., Jäättelä, M., Jackson, W.T., Jiang, X., Jin, S., Johansen, T., Jung, J.U., Kadowaki, M., Kang, C., Kelekar, A., Kessel, D.H., Kiel, J.A.K.W., Kim, H.P., Kimchi, A., Kinsella, T.J., Kiselyov, K., Kitamoto, K., Knecht, E., Komatsu, M., Kominami, E., Kondo, S., Kovács, A.L., Kroemer, G., Kuan, C.-Y., Kumar, R., Kundu, M., Landry, J., Laporte, M., Le, W., Lei, H.-Y., Lenardo, M.J., Levine, B., Lieberman, A., Lim, K.-L., Lin, F.-C., Liou, W., Liu, L.F., Lopez-Berestein, G., López-Otín, C., Lu, B., Macleod, K.F., Malorni, W., Martinet, W., Matsuoka, K., Mautner, J., Meijer, A.J., Meléndez, A., Michels, P., Miotto, G., Mistiaen, W.P., Mizushima, N., Mograbi, B., Monastyrska, I., Moore, M.N., Moreira, P.I., Moriyasu, Y., Motyl, T., Münz, C., Murphy, L.O., Naqvi, N.I., Neufeld, T.P., Nishino, I., Nixon, R.A., Noda, T., Nürnberg, B., Ogawa, M., Oleinick, N.L., Olsen, L.J., Ozpolat, B., Paglin, S., Palmer, G.E., Papassideri, I., Parkes, M., Perlmutter, D.H., Perry, G., Piacentini, M., Pinkas-Kramarski, R., Prescott, M., Proikas-Cezanne, T., Raben, N., Rami, A., Reggiori, F., Rohrer, B., Rubinsztein, D.C., Ryan, K.M., Sadoshima, J., Sakagami, H., Sakai, Y., Sandri, M., Sasakawa, C., Sass, M., Schneider, C., Seglen, P.O., Seleverstov, O., Settleman, J., Shacka, J.J., Shapiro, I.M., Sibirny, A., Silva-Zacarin, E.C.M., Simon, H.-U., Simone, C., Simonsen, A., Smith, M.A., Spanel-Borowski, K., Srinivas, V., Steeves, M., Stenmark, H., Stromhaug, P.E., Subauste, C.S., Sugimoto, S., Sulzer, D., Suzuki, T., Swanson, M.S., Tabas, I., Takeshita, F., Talbot, N.J., Tallóczy, Z., Tanaka, Keiji, Tanaka, Kozo, Tanida, I., Taylor, G.S., Taylor, J.P., Terman, A., Tettamanti, G., Thompson, C.B., Thumm, M., Tolkovsky, A.M., Tooze, S.A., Truant, R., Tumanovska, L.V., Uchiyama, Y., Ueno, T., Uzcátegui, N.L., van der Klei, I., Vaquero, E.C., Vellai, T., Vogel, M.W., Wang, H.-G., Webster, P., Wiley, J.W., Xi, Z., Xiao, G., Yahalom, J., Yang, J.-M., Yap, G., Yin, X.-M., Yoshimori, T., Yu, L., Yue, Z., Yuzaki, M., Zabirnyk, O., Zheng, X., Zhu, X., Deter, R.L., 2008. Guidelines for the use and interpretation of assays for monitoring autophagy in higher eukaryotes. Autophagy 4, 151–175. https://doi.org/10.4161/auto.5338.

Klionsky, D.J., Abeliovich, H., Agostinis, P., Agrawal, D.K., Aliev, G., Askew, D.S., Baba, M., Baehrecke, E.H., Bahr, B.A., Ballabio, A., Bamber, B.A., Bassham, D.C., Bergamini, E., Kroemer, G., Kuan, C., Kumar, R., Kundu, M., Landry, J., Laporte, M., Le, W., Lei, H., Michael, J., Levine, B., Lieberman, A., Lim, K., Lin, F., Liou, W., Liu, L.F., Lopez-berestein, G., López-otín, C., Macleod, K.F., Malorni, W., Martinet, W., Matsuoka, K., Mistiaen, W.P., Mizushima, N., Mograbi, B., Münz, C., Murphy, L.O., Naqvi, N.I., Thomas, P., Ogawa, M., Oleinick, N.L., Olsen, L.J., Ozpolat, B., Perry, G., Piacentini, M., Pinkas-kramarski, R., 2009. Guidelines for the use and interpretation of assays for monitoring autophagy in higher eukaryotes. Autophagy 4, 151–175.

Kraemer, B.C., Schuck, T., Wheeler, J.M., Robinson, L.C., Trojanowski, J.Q., Lee, V.M.Y., Schellenberg, G.D., 2010. Loss of murine TDP-43 disrupts motor function and plays an essential role in embryogenesis. Acta Neuropathol. 119, 409–419. https://doi.org/10.1007/s00401-010-0659-0.

Langellotti, S., Romano, V., Romano, G., Klima, R., Feiguin, F., Cragnaz, L., Romano, M., Baralle, F.E., 2016. A novel Drosophila model of TDP-43 proteinopathies: N-terminal sequences combined with the Q/N domain induce protein functional loss and locomotion defects. Dis. Model. Mech. 9, 659–669. https://doi.org/10.1242/dmm.023382.

Lee, E.B., Lee, V.M.-Y., Trojanowski, J.Q., 2011. Gains or losses: molecular mechanisms of TDP43-mediated neurodegeneration. Nat. Rev. Neurosci. 13, 38–50. https://doi.org/10.1038/nrn3121.

Ling, S.-C., Polymenidou, M., Cleveland, D.W., 2013. Converging mechanisms in ALS and FTD: disrupted RNA and protein homeostasis. Neuron 79, 416–438. https://doi.org/10.1016/j.neuron.2013.07.033.

Ling, J.P., Pletnikova, O., Troncoso, J.C., Wong, P.C., 2015. TDP-43 repression of nonconserved cryptic exons is compromised in ALS-FTD. Science 349, 650–655. https://doi.org/10.1126/science.aab0983.

Mackenzie, I.R., Rademakers, R., Neumann, M., 2010. TDP-43 and FUS in amyotrophic lateral sclerosis and frontotemporal dementia. Lancet Neurol. 9, 995–1007. https://doi.org/10.1016/S1474-4422(10)70195-2.

Margiotta, A., 2021. Role of SNAREs in neurodegenerative diseases. Cells 10. https://doi.org/10.3390/cells10050991.
Miller, R.G., Mitchell, J.D., Moore, D.H., 2012. Riluzole for amyotrophic lateral sclerosis (ALS)/motor neuron disease (MND). Cochrane Database Syst. Rev. CD001447. https://doi.org/10.1002/14651858.CD001447.pub3.
Nadanaciva, S., Lu, S., Gebhard, D.F., Jessen, B.A., Pennie, W.D., Will, Y., 2011. A high content screening assay for identifying lysosomotropic compounds. Toxicol. in Vitro 25, 715–723. https://doi.org/10.1016/j.tiv.2010.12.010.
Nedelsky, N.B., Todd, P.K., Taylor, J.P., 2008. Autophagy and the ubiquitin-proteasome system: collaborators in neuroprotection. Biochim. Biophys. Acta 1782, 691–699. https://doi.org/10.1016/j.bbadis.2008.10.002.
Neumann, M., Sampathu, D.M., Kwong, L.K., Truax, A.C., Micsenyi, M.C., Chou, T.T., Bruce, J., Schuck, T., Grossman, M., Clark, C.M., McCluskey, L.F., Miller, B.L., Masliah, E., Mackenzie, I.R., Feldman, H., Feiden, W., Kretzschmar, H.A., Trojanowski, J.Q., Lee, V.M.-Y., 2006. Ubiquitinated TDP-43 in frontotemporal lobar degeneration and amyotrophic lateral sclerosis. Science (New York, N.Y.) 314, 130–133. https://doi.org/10.1126/science.1134108.
Nishimura, A.L., Župunski, V., Troakes, C., Kathe, C., Fratta, P., Howell, M., Gallo, J., Hortobágyi, T., Shaw, C.E., Rogelj, B., 2010. Nuclear import impairment causes cytoplasmic trans-activation response DNA-binding protein accumulation and is associated with frontotemporal lobar degeneration. Brain 133, 1763–1771. https://doi.org/10.1093/brain/awq111.
Nonaka, T., Masuda-Suzukake, M., Arai, T., Hasegawa, Y., Akatsu, H., Obi, T., Yoshida, M., Murayama, S., Mann, D.M.A., Akiyama, H., Hasegawa, M., 2013. Prion-like properties of pathological TDP-43 aggregates from diseased brains. Cell Rep. 4, 124–134. https://doi.org/10.1016/j.celrep.2013.06.007.
Pilkington, G.J., Akinwunmi, J., Amar, S., 2006. The role of tricyclic drugs in selective triggering of mitochondrially-mediated apoptosis in neoplastic glia : a therapeutic option in malignant glioma ? Radiol. Oncol. 40, 73–85.
Ratti, A., Buratti, E., 2016. Physiological functions and pathobiology of TDP-43 and FUS/TLS proteins. J. Neurochem. 138, 95–111. https://doi.org/10.1111/jnc.13625.
Romano, G., Klima, R., Buratti, E., Verstreken, P., Baralle, F.E., Feiguin, F., 2014. Chronological requirements of TDP-43 function in synaptic organization and locomotive control. Neurobiol. Dis. 71, 95–109. https://doi.org/10.1016/j.nbd.2014.07.007.
Rossi, M., Munarriz, E.R., Bartesaghi, S., Milanese, M., Dinsdale, D., Guerra-Martin, M.A., Bampton, E.T.W., Glynn, P., Bonanno, G., Knight, R.A., Nicotera, P., Melino, G., 2009. Desmethylclomipramine induces the accumulation of autophagy markers by blocking autophagic flux. J. Cell Sci. 122, 3330–3339. https://doi.org/10.1242/jcs.048181.
Rothstein, J.D., 2017. Edaravone: a new drug approved for ALS. Cell 171, 725. https://doi.org/10.1016/j.cell.2017.10.011.
Scotter, E.L., Vance, C., Nishimura, A.L., Lee, Y.-B., Chen, H.-J., Urwin, H., Sardone, V., Mitchell, J.C., Rogelj, B., Rubinsztein, D.C., Shaw, C.E., 2014. Differential roles of the ubiquitin proteasome system and autophagy in the clearance of soluble and aggregated TDP-43 species. J. Cell Sci. 127, 1263–1278. https://doi.org/10.1242/jcs.140087.
Sephton, C.F., Good, S.K., Atkin, S., Dewey, C.M., Mayer, P., Herz, J., Yu, G., 2010. TDP-43 is a developmentally regulated protein essential for early embryonic development. J. Biol. Chem. 285, 6826–6834. https://doi.org/10.1074/jbc.M109.061846.
Shiga, A., Ishihara, T., Miyashita, A., Kuwabara, M., Kato, T., Watanabe, N., Yamahira, A., Kondo, C., Yokoseki, A., Takahashi, M., Kuwano, R., Kakita, A., Nishizawa, M., Takahashi, H., Onodera, O., 2012. Alteration of POLDIP3 splicing associated with loss of function of TDP-43 in tissues affected with ALS. PLoS One 7, e43120. https://doi.org/10.1371/journal.pone.0043120.
Silani, V., Ludolph, A., Fornai, F., 2017. The emerging picture of ALS: a multisystem, not only a “motor neuron disease”. Arch. Ital. Biol. 155, 99–109, 10.12871/00039829201741.
Smethurst, P., Newcombe, J., Troakes, C., Simone, R., Chen, Y.-R., Patani, R., Sidle, K., 2016. In vitro prion-like behaviour of TDP-43 in ALS. Neurobiol. Dis. 96, 236–247. https://doi.org/10.1016/j.nbd.2016.08.007.
Sreedharan, J., Blair, I.P., Tripathi, V.B., Hu, X., Vance, C., Rogelj, B., Ackerley, S., Durnall, J.C., Williams, K.L., Buratti, E., Baralle, F., de Belleroche, J., Mitchell, J.D., Leigh, P.N., Al-Chalabi, A., Miller, C.C., Nicholson, G., Shaw, C.E., 2008. TDP-43 mutations in familial and sporadic amyotrophic lateral sclerosis. Science 319, 1668–1672. https://doi.org/10.1126/science.1154584.
Stavrovskaya, I.G., Narayanan, M. V, Zhang, W., Krasnikov, B.F., Heemskerk, J., Young, S.S., Blass, J.P., Brown, A.M., Beal, M.F., Friedlander, R.M., Kristal, B.S., 2004. Clinically approved heterocyclics act on a mitochondrial target and reduce stroke-induced pathology. J. Exp. Med. 200, 211–222. 10.1084/jem.20032053.
Tamaki, Y., Shodai, A., Morimura, T., Hikiami, R., Minamiyama, S., Ayaki, T., Tooyama, I., Furukawa, Y., Takahashi, R., Urushitani, M., 2018. Elimination of TDP-43 inclusions linked to amyotrophic lateral sclerosis by a misfolding-specific intrabody with dual proteolytic signals. Sci. Rep. 8, 1–16. https://doi.org/10.1038/s41598-018-24463-3.
Taylor, J.P., Brown, R.H., Cleveland, D.W., 2016. Decoding ALS: from genes to mechanism. Nature 539, 197–206. https://doi.org/10.1038/nature20413.
Torrente, M.P., Chuang, E., Noll, M.M., Jackrel, M.E., Go, M.S., Shorter, J., 2016. Mechanistic insights into Hsp104 potentiation. J. Biol. Chem. 291, 5101–5115. https://doi.org/10.1074/jbc.M115.707976.
Tsvetkov, A.S., Miller, J., Arrasate, M., Wong, J.S., Pleiss, M.A., Finkbeiner, S., 2010. A small-molecule scaffold induces autophagy in primary neurons and protects against toxicity in a Huntington disease model. Proc. Natl. Acad. Sci. U. S. A. 107, 16982–16987. https://doi.org/10.1073/pnas.1004498107.
Van Damme, P., Dewil, M., Robberecht, W., Van Den Bosch, L., 2005. Excitotoxicity and amyotrophic lateral sclerosis. Neurodegener. Dis. 2, 147–159. https://doi.org/10.1159/000089620.
Walker, A.K., Spiller, K.J., Ge, G., Zheng, A., Xu, Y., Zhou, M., Tripathy, K., Kwong, L.K., Trojanowski, J.Q., Lee, V.M.-Y., 2015. Functional recovery in new mouse models of ALS/FTLD after clearance of pathological cytoplasmic TDP-43. Acta Neuropathol. https://doi.org/10.1007/s00401-015-1460-x.
Wegorzewska, I., Baloh, R.H., 2011. TDP-43-based animal models of neurodegeneration: new insights into ALS pathology and pathophysiology. Neurodegener. Dis. 8, 262–274. https://doi.org/10.1159/000321547.
Winton, M.J., Van Deerlin, V.M., Kwong, L.K., Yuan, W., Wood, E.M., Yu, C.-E., Schellenberg, G.D., Rademakers, R., Caselli, R., Karydas, A., Trojanowski, J.Q., Miller, B.L., Lee, V.M.-Y., 2008. A90V TDP-43 variant results in the aberrant localization of TDP-43 in vitro. FEBS Lett. 582, 2252–2256. https://doi.org/10.1016/j.febslet.2008.05.024.
Wu, M.N., Fergestad, T., Lloyd, T.E., He, Y., Broadie, K., Bellen, H.J., 1999. Syntaxin 1A interacts with multiple exocytic proteins to regulate neurotransmitter release in vivo. Neuron 23, 593–605. https://doi.org/10.1016/s0896-6273(00)80811-9.
Yang, C., Wang, H., Qiao, T., Yang, B., Aliaga, L., Qiu, L., Tan, W., Salameh, J., McKenna-Yasek, D.M., Smith, T., Peng, L., Moore, M.J., Brown, R.H., Cai, H., Xu, Z., 2014. Partial loss of TDP-43 function causes phenotypes of amyotrophic lateral sclerosis. PNAS 111, E1121–E1129. https://doi.org/10.1073/pnas.1322641111.
Yoshii, S.R., Mizushima, N., 2017. Monitoring and measuring autophagy. Int. J. Mol. Sci. 18 https://doi.org/10.3390/ijms18091865.
Zhang, Y.-J., Gendron, T.F., Xu, Y.-F., Ko, L.-W., Yen, S.-H., Petrucelli, L., 2010. Phosphorylation regulates proteasomal-mediated degradation and solubility of TAR DNA binding protein-43 C-terminal fragments. Mol. Neurodegener. 5, 33. https://doi.org/10.1186/1750-1326-5-33.
Zhang, Y.-J., Caulfield, T., Xu, Y.-F., Gendron, T.F., Hubbard, J., Stetler, C., Sasaguri, H., Whitelaw, E.C., Cai, S., Lee, W.C., Petrucelli, L., 2013. The dual functions of the extreme N-terminus of TDP-43 in regulating its biological activity and inclusion formation. Hum. Mol. Genet. 22, 3112–3122. https://doi.org/10.1093/hmg/ddt166.